

**ANALYTICAL SOLUTION FOR MECHANICAL
STRESSES OF MULTILAYERED
HOLLOW SPHERICAL PRESSURE VESSEL**

NG YEE PING


**A project report submitted in partial fulfilment of the
requirements for the award of Bachelor of Engineering
(Honours) Mechanical Engineering**

**Lee Kong Chian Faculty of Engineering and Science
Universiti Tunku Abdul Rahman**

May 2020

DECLARATION

I hereby declare that this project report is based on my original work except for citations and quotations which have been duly acknowledged. I also declare that it has not been previously and concurrently submitted for any other degree or award at UTAR or other institutions.

Signature : 

Name : Ng Yee Ping

ID No. : 1506297

Date : 15 May 2020

APPROVAL FOR SUBMISSION

I certify that this project report entitled “**ANALYTICAL SOLUTION FOR MECHANICAL STRESSES OF MULTILAYERED HOLLOW SPHERICAL PRESSURE VESSEL**” was prepared by **NG YEE PING** has met the required standard for submission in partial fulfilment of the requirements for the award of Bachelor of Engineering (Honours) Mechanical Engineering at Universiti Tunku Abdul Rahman.

Approved by,

Signature

:



Supervisor

:

Dr Yeo Wei Hong

Date

:

15/5/20

The copyright of this report belongs to the author under the terms of the copyright Act 1987 as qualified by Intellectual Property Policy of Universiti Tunku Abdul Rahman. Due acknowledgement shall always be made of the use of any material contained in, or derived from, this report.

© 2020, Ng Yee Ping. All right reserved.

ACKNOWLEDGEMENTS

I would like to thank everyone who had contributed to the successful completion of this project. First of all, I would like to express my gratitude to my research supervisor, Dr Yeo for his invaluable advice, guidance and his unwavering patience throughout the development of the research.

In addition, I would also like thank my loving family and my loyal friends who had given me the courage to proceed in this research project, even in the face of numerous challenges.

ABSTRACT

Pressure vessels are enclosed devices typically used to store fluids under very high pressure. Some common applications include BBQ butane grills, LPG tanks, and oil tankers. For the past decades, multilayered and FGM pressure vessels have increased in popularity due to their superior strength without adding bulk to the vessel itself. The design of these pressure vessels has to be complemented with an accurate prediction of its mechanical stress distributions while under load. Over the years, several methods have been proposed to develop solutions to accomplish this, most of which employ the use of numerical methods in the solutions. No study thus far has proposed a fully analytical solution that specializes in the stress behaviour of multilayered spherical pressure vessels. Therefore, for this project, an analytical solution was developed via the recursive method for the displacement and the stress performance of a multilayered hollow sphere. The basis of this solution is adapted from the stress-strain relationship equations for spheres, as well as the equilibrium equation. This analytical solution was then programmed into MATLAB. For verification purposes, the results from this proposed solution were compared to both the results from a Finite Element Analysis, as well as the results published in literature. The proposed solution has generated results that were in nearly complete agreement with the results from the reference paper as well as the FEA outcome. Overall, the average values of the percentage errors are: 0.5% for the comparison with the FEA simulation, and 1.5% for the comparison with the reference paper. It is also found that the optimal number of layers to be modelled for FGM structures is 500 layers.

TABLE OF CONTENTS

DECLARATION		i
APPROVAL FOR SUBMISSION		ii
ACKNOWLEDGEMENTS		iv
ABSTRACT		v
TABLE OF CONTENTS		vi
LIST OF TABLES		viii
LIST OF FIGURES		ix
LIST OF SYMBOLS / ABBREVIATIONS		xii
LIST OF APPENDICES		xiii
CHAPTER		
1	INTRODUCTION	1
1.1	General Introduction	1
1.2	Importance of the Study	1
1.3	Problem Statement	2
1.4	Aim and Objectives	3
1.5	Scope and Limitation of the Study	3
1.6	Contribution of the Study	4
1.7	Outline of the Report	4
2	LITERATURE REVIEW	5
2.1	Introduction to Pressure Vessels	5
2.2	The Structural Integrity of Pressure Vessels	5
2.3	Pressure Vessels with Modern Material Choices	6
2.4	Stress-strain Equations for Spheres	8
2.5	Finite Element Analyses of Pressure Vessels	11
2.6	Summary	14
3	METHODOLOGY AND WORK PLAN	15
3.1	Introduction	15
3.2	Development of the Solution	15

3.3	Computational Procedures for the Solution	21
3.4	Geometry, Material Properties, and Boundary Conditions	22
3.4.1	Initializing	25
3.4.2	Geometry	27
3.4.3	Model	31
3.4.4	Execution and Data Retrieval	36
3.5	Summary	37
4	RESULTS AND DISCUSSION	38
4.1	Introduction	38
4.2	Results Verification	38
4.2.1	Results Verification with Literature	38
4.2.2	Results Verification with FEA Outcome	40
4.3	Convergence Study	42
4.4	Parametric Study	46
4.4.1	Varying the Elastic Modulus	47
4.4.2	Varying the Loading Pressure	49
4.4.3	Varying the Wall Thickness	50
4.5	Observations from the Study	52
5	CONCLUSIONS AND RECOMMENDATIONS	54
5.1	Conclusions	54
5.2	Recommendations for Future Work	55
	REFERENCES	56
	APPENDICES	59

LIST OF TABLES

TABLE	TITLE	PAGE
A-1	Comparison between the Proposed Analytical Solution and the Reference Solution for the Linear Displacement.	59
A-2	Comparison between the Proposed Analytical Solution and the Reference Solution for the Normalized Radial Stress.	60
A-3	Comparison between the Proposed Analytical Solution and the Reference Solution for the Normalized Tangential Stress.	61
A-4	Comparison between the Proposed Analytical Solution and the Finite Element Analysis for the Linear Displacement.	62
A-5	Comparison between the Proposed Analytical Solution and the Finite Element Analysis for the Normalized Radial Stress.	63
A-6	Comparison between the Proposed Analytical Solution and the Finite Element Analysis for the Normalized Tangential Stress.	64

LIST OF FIGURES

FIGURE	TITLE	PAGE
2.1	Sectional View of a Piezoelectric Multilayered Sphere (Khorsand & Tang, 2019).	8
2.2	(a) the Geometrical Data and Notations for a 3D Shell Model, and (b) Different Geometries Achievable via Modifying the Reference System (Brischetto, 2017).	11
2.3	(a) A Single-layered Hollow Sphere in Axisymmetric Configuration, and (b) A Zoomed-in View of the Model (Li, et al., 2012).	11
2.4	(a) A 2D FEA Model, and (b) Demonstration of Meshing Priorities (Somadder & Islam, 2015).	12
2.5	Comparison between the Analytical Solution and the FEA Solution for the (a) Radial Stress, and (b) Hoop Stress (Zhang, et al., 2012).	13
3.1	A Sketch of the 2D FEA Model.	24
3.2	The Main Window.	25
3.3	The Engineering Data Page.	26
3.4	Creating a New Geometry via DesignModeler.	27
3.5	Selecting “Look At Face” at the Upper Right Corner.	27
3.6	Outlining a Semi-hemisphere.	28
3.7	Generating a Body from the Sketch.	28
3.8	Creating a New Sketch to Sketch the Layer Interfaces.	29
3.9	Selecting “Slice Material” to Cut the Body into Different Layers.	29
3.10	The Finalized Sketch of a Multilayered Sphere.	30
3.11	Configuring the System as Axisymmetric.	31
3.12	Setting Up a Construction Geometry.	31

FIGURE	TITLE	PAGE
3.13	Inserting a Path.	32
3.14	Defining the Path.	32
3.15	Constraining the Mesh by its Sizing.	33
3.16	Generating the Mesh with a Predefined Element Size.	33
3.17	Defining the Loading Conditions.	34
3.18	Defining the Inner and Outer Pressures.	34
3.19	Constraining the Displacement in the Y-direction.	35
3.20	Confining the Simulation on the Path Created.	36
3.21	Exporting the Data.	36
3.22	The Data Extracted from the FEA.	37
4.1	Graphs Plotted for the Analytical Solution and the Results Produced by Bayat for (a) Linear Displacement, (b) Radial Stress, and (c) Tangential Stress.	39
4.2	Graphs Plotted for the Analytical Solution and the Results Produced by the FEA for (a) Linear Displacement, (b) Radial Stress, and (c) Tangential Stress.	41
4.3	Graphs Plotted for the Analytical Solution (50 layered) and the Results Produced by Bayat et al. (2011) for (a) Linear Displacement, (b) Radial Stress, and (c) Tangential Stress.	43
4.4	Graphs Plotted for the Analytical Solution (500 layered) and the Results Produced by the FEA for (a) Linear Displacement, (b) Radial Stress, and (c) Tangential Stress.	45
4.5	The Effects of an Increasing Elastic Modulus on the Graph of Linear Displacement against Thickness Ratio.	47
4.6	The Effects of an Increasing Elastic Modulus on the Graph of Normalized Radial Stress against Thickness Ratio.	48

FIGURE	TITLE	PAGE
4.7	The Effects of an Increasing Elastic Modulus on the Graph of Normalized Tangential Stress against Thickness Ratio.	49
4.8	The Effects of an Increasing Load on the Graph of Linear Displacement against Thickness Ratio.	50
4.9	The Effects of Varying Wall Thickness for the Graphs of (a) Linear Displacement, (b) Normalized Radial Stress, and (c) Normalized Tangential Stress.	51

LIST OF SYMBOLS / ABBREVIATIONS

CFM	Complementary Functions Method
FEA	Finite Element Analysis
FGM	Functionally Graded Material
RK5	Runge-Kutta Method of the 5 th Order
r_i	Radius at layer i
$\sigma_{rr,i}(r)$	Radial stress at layer i
$\sigma_{\phi\phi,i}(r)$	Tangential / circumferential stress at layer i
$\varepsilon_{rr,i}$	Radial strain at layer i
$\varepsilon_{\phi\phi,i}$	Tangential / circumferential strain at layer i
$u_{r,i}(r)$	Linear displacement at layer i
E_i	Elastic Modulus for the material at layer i
ν_i	Poisson ratio for the material at layer i
q_i	Contact pressure at layer i
P_{int}	Internal pressure exerted on the pressure vessel
P_{ext}	External pressure exerted on the pressure vessel

LIST OF APPENDICES

APPENDIX	TITLE	PAGE
A	Results Verification Comparisons	59
B	Originality Report	66
C	Comment on Originality Report	67

CHAPTER 1

INTRODUCTION

1.1 General Introduction

A pressure vessel refers to a container whose internals are maintained at a pressure different from the ambient pressure (Livingston & Scavuzzo, 2000). A pressure vessel is most commonly used for the purpose of transportation and storage of compressible fluids, usually gases. Since the volume of a fluid is inversely proportional to its pressure, fluids are usually pressurized to a fraction of its original volume (at atmospheric pressure) and stored inside a container. This container is deemed the pressure vessel.

Over the years, the use of pressure vessels as gas containers has become more and more widespread across varying fields. As a result, these pressure vessels have specialized into their respective niches, depending on their use case. There are now a variety of pressure vessels in a multitude of different shapes and sizes.

A specialized container is needed for the storage and transportation of such pressurized gases, simply because the gases within the containers are under very high pressure, usually high enough to cause a fatal accident if the container fails. Other than that, the contents within pressure vessels can also be highly flammable, corrosive, biohazardous, or even radioactive. Thus, it is of utmost importance that pressure vessels can reliably store these chemicals and be able to withstand the test of time (Dubal & Kadam, 2017). A well-built pressure vessel should allow no significant leakage of stored material to the surroundings.

1.2 Importance of the Study

Pressure vessels, as the name implies, are constantly under pressure while under operation. This pressure comes from two sources: mechanical stresses and thermal stresses. These stresses originate from the pressurized content it is carrying, as well as environmental stresses.

For vessels carrying material at extremely high temperatures, it is not surprising to find the magnitude of the thermal stresses exceed the mechanical stresses occasionally (Darijani, et al., 2009). Therefore, it is important to ensure

these pressure vessels are not overloaded, for it will lead to grave consequences otherwise.

A comprehensive study of the stress distribution of pressure vessels under a certain load could prevent this from happening. With a clear understanding of the required specifications and the behaviour of the vessel under these loads, a properly designed pressure vessel can be assigned to the task. This has given rise to a need for a more precise approximation for these situations.

1.3 Problem Statement

There has been a number of published mathematical solutions regarding the mechanical stresses in multilayered pressure vessels. However, there is a noticeably fewer number of papers focused on spherical vessels. Owing to its higher popularity, cylindrical vessels were more often studied.

Among the studies carried out on multilayered spherical vessels, some of them relied on differential equations for their final outcome, while the rest of the papers have incorporated various numerical methods into their solutions.

Numerical solutions are well suited for these applications. Usually, numerical methods are adopted to reduce the initial mathematical models into simpler forms to allow for quicker and more reliable results with the help of computers. Assumptions were usually made to ease this process. In the process of doing so, a certain degree of accuracy is inevitably sacrificed for the sake of convenience (Brownlee, 2018).

No study thus far has proposed a fully analytical solution that specializes in the stress behaviour of multilayered spherical pressure vessels.

1.4 Aim and Objectives

The aim of this project is to develop a complete analytical solution that is capable of accurately predicting the mechanical stress distribution of multilayered hollow spherical pressure vessels.

To achieve this aim, several objectives have been established:

- To derive the analytical solution for the mechanical stresses of a spherical pressure vessel, starting from the stress-strain relation equations for spherical structures.
- To program the solution into MATLAB and run the solution with a predefined set of material properties and loading conditions.
- To verify the accuracy of the proposed solution by comparing it to the results obtained from a 2D FEA simulation, as well as a set of reference results from a suitable and reliable external source.

1.5 Scope and Limitation of the Study

This project focuses on the development of an analytical solution to solve for the stresses in spherical pressure vessels. Therefore, this solution will not be applicable to vessels of different shapes due to their distinct geometry.

As mentioned above, the stresses undergone by the pressure vessels are composed of two separate sources: mechanical and thermal stresses. However, for the sake of simplicity, only the mechanical stress was considered in the proposed solution for this project. This will allow for a reduction in the complexity of the solution. This limitation is expected to contribute to a reduced accuracy if the subject of study does not ignore the thermal effects.

1.6 Contribution of the Study

By the end of this project, an analytical solution for the mechanical stresses of a multilayered spherical pressure vessel will be proposed and tested. This solution will be specialized in spherical pressure vessels made of multiple layers of distinct mechanical properties. The parameters important in the design of pressure vessels will be reviewed to observe their effects on the performance of these vessels. This data would give a better understanding on how the changes in properties will affect the mechanical stresses in a pressure vessel.

1.7 Outline of the Report

For the following Chapter 2 in this report, a literature study would be performed on pressure vessels, the stress distribution of pressure vessels, and the numerous ways that can be used to model for a spherical pressure vessel. In Chapter 3, the derivation of the analytical solution will be discussed, accompanied by the procedures taken while modelling for a hollow sphere in ANSYS. The findings of this project will be discussed in detail in Chapter 4, including a convergence study as well as a parametric study. This report will be concluded with Chapter 5, along with some recommendations for future work to be done.

CHAPTER 2

LITERATURE REVIEW

2.1 Introduction to Pressure Vessels

After more than a century of innovations, there is a vast portfolio of pressure vessels of various sizes and shapes. In this day and age, pressure vessels can be seen in almost any corner of the planet from the domestic LPG barrels to the industrial-grade vessels used in petrochemical plants.

Pressure vessels are generally divided into categories based on their general shape. Theoretically, pressure vessels of any shape could be built. However, there are rarely any pressure vessels made for commercial use that is not either cylindrical or spherical in shape, simply because vessels with odd shapes have much more complicated geometry (Mukherjee, 2019). This makes them difficult to manufacture, and also difficult to be modelled to study their performance. Oddly shaped structures are also more difficult to strengthen due to a prevalence of stress concentration points (Zheng, et al., 2019). As a result, commercial pressure vessels have mostly remained either cylindrical or spherical in shape.

2.2 The Structural Integrity of Pressure Vessels

As a whole, pressure vessels are heavy-duty appliances that are designed to last for prolonged periods of time while being subjected to strenuous environments. This is due to the harmful or even life-threatening situations that might happen if a pressure vessel loses its structural integrity.

According to Thomson (2015), in the nineteenth and twentieth centuries, the safety and reliability of the boilers used in the United States were in no way guaranteed. Explosions happened frequently, alongside the fatalities that they caused. Between the years 1992 and 2001, a total of 23,338 pressure vessel related accidents were reported in the United Kingdom alone. This averages out to 2,334 accidents a year. Among them, the year 2000 saw the highest record at 2,686 accidents. Fatalities from these accidents were recorded at 127 deaths from the years 2000 to 2010 (Mukherjee, 2019).

Usually, failures in pressure vessels happen slowly and can be easily detected by process monitors (Khorsand & Tang, 2019). There is also plenty of factors that can contribute to such a failure, whether directly or indirectly. Some of these factors include the presence of stress concentration factors in the geometry of the vessel, the use of low-quality alloys in the vessel, corrosion of the body by the fluids contained within, fatigue damage from cyclic loading, or even operator failure (Zheng, et al., 2019). Fortunately, accidents of this nature are unlikely to occur in this day and age, as long as the operators exercise due diligence and report any irregularities that may snowball into larger problems down the road.

2.3 Pressure Vessels with Modern Material Choices

As the years have passed, the loading pressure in pressure vessels have skyrocketed. The motivation behind these ever-increasing demands is, as usual, driven by cost saving measures. Higher operating pressures lead to a smaller pressure vessel, which contributes to cost savings by saving space.

As a result of this trend, traditional single layered pressure vessels are no longer structurally strong enough to withstand the high loading stresses for an extended period of time. From there, multilayered pressure vessels were born. Each layer was meant to be tailor-made to the stresses that it was expected to be under. Appropriate material choices were to be carefully made for each layer, as well as the laminates that accompany each layer (Zhang, et al., 2012). Thus, pressure vessels made of either multilayered materials or functionally graded materials have increased in popularity.

Structures made of functionally graded materials (FGM) are noteworthy because of its varying mechanical properties across its depth (Moita, et al., 2019). They are generally classified as composite materials, but instead of being made up of several distinct layers of material, there is a gradient along its radial direction where its properties slowly transition from one form into the other.

According to Kashtalyan (2004), FGMs are mostly made of different materials fused together via powder metallurgy manufacturing processes. The concept behind FGMs was initially developed with the advancement of super heat resistant materials in mind. The main intention behind the development of FGMs was for it to be implemented in nuclear reactors. This technology

eventually trickled down to be adopted in pressure vessels, among other applications involving heightened temperatures over long periods of time.

Moreover, simply by varying the material as well as its concentration gradient, FGMs can be engineered to suit a wide variety of industrial applications (Tutuncu & Ozturk, 2001). Using appropriate ferromagnetic materials, Dai et al. (2010) has even managed to model for the fluctuations in the magnetic field vector in a spherical FGM hollow sphere. This has proven the flexibility of FGMs when employed in pressure vessels.

Bayat et al (2011) has even claimed that the increase in demand for vessels with higher sustainable pressure has resulted in a significant spike in demand for modern FGM pressure vessels. FGM Pressure vessels are usually preferred to both fiber-reinforced and laminated composite materials. The reason being the continuous change in the microstructure in FGMs are less likely to be subjected to a mismatch of mechanical properties across the interface, which is a problem in reinforced or laminated materials. As an added benefit, FGMs can also be used to mitigate stress concentrations when a thin layer of FGM material is coated onto the surface of a structure made of a homogeneous material (Zheng, et al., 2019).

On the other hand, there are multilayered pressure vessels. Multilayered pressure vessels differ from FGM pressure vessels on one crucial aspect. Instead of having a gradual variation in the mechanical properties along its thickness direction, multilayered pressure vessels are simply made up of two or more distinct layers on top of one another.

Similar to FGM pressure vessels, multilayered vessels also have access to a wide variety of materials for the construction of its individual layers, so that each layer can be tailored to the stresses it is expected to endure, thus significantly increasing its overall strength and durability.

One issue with multilayered pressure vessels is the fact that the boundaries between these layers suffer from a mismatch in their mechanical properties, particularly the elastic modulus and the Poisson's ratio. A stress discontinuity is used to describe the situation at these interfaces (Zhang, et al., 2012).

There are also multilayered vessels whose outermost layer are made of piezoelectric materials as shown in Figure 2.1 below. Piezoelectric panels

generate electric charge when put under mechanical stress. This allows the vessel to output its stress levels to be monitored during its operation. The constant monitoring of these data can be used to determine the health of the pressure vessel to avoid failures.

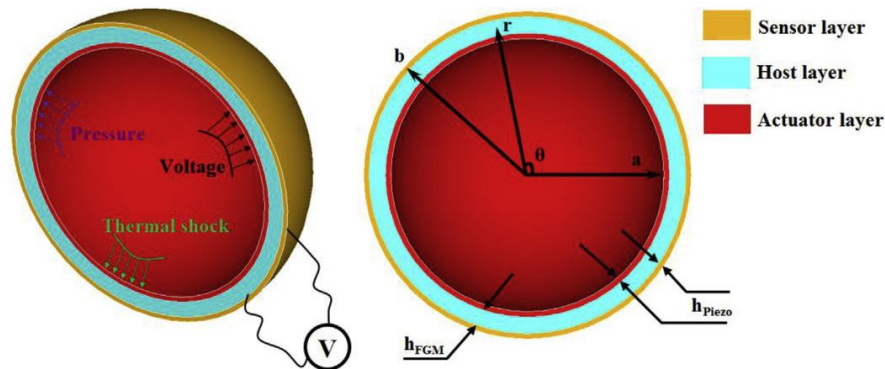


Figure 2.1: Sectional View of a Piezoelectric Multilayered Sphere (Khorsand & Tang, 2019).

2.4 Stress-strain Equations for Spheres

During the design process, the viability of a pressure vessel has to be evaluated by simulating its stress-strain performance when put under an operating load. There are many ways to approach this, and the most obvious way is to carry out a Finite Element Analysis (FEA) with the aid of an appropriate software suite.

However, mathematical models for stress-strain calculations are usually preferred to simulations, simply because they are less time consuming. Since saved time equals saved costs, various analytical solutions are more widely used by professionals as opposed to running simulations for each and every configuration during their design process (Somadder & Islam, 2015).

Developing a mathematical model for a FGM pressure vessel is a challenge due to its continually varying mechanical properties. To work around this limitation, one common practice among researchers is to develop algorithms for multilayered vessels instead. The FGM vessel is then modelled as a multilayered vessel with N number of layers (Shi, et al., 2006).

The development of these solutions typically begins at the basic stress-strain relations. These are well established, well documented equations that can

be applied to most situations involving spherical structures in the world of solid mechanics:

$$\varepsilon_{rr,i} = \frac{1}{E_i} [\sigma_{rr,i} - 2\nu\sigma_{\phi\phi,i}] \quad (2.1a)$$

$$\varepsilon_{\phi\phi,i} = \frac{1}{E_i} [(1 - \nu)\sigma_{\phi\phi,i} - \nu\sigma_{rr,i}] \quad (2.1b)$$

with the equilibrium equation as follows:

$$\frac{d}{dr}(\sigma_{rr,i}) + \frac{2(\sigma_{rr,i} - \sigma_{\phi\phi,i})}{r} \quad (2.2)$$

From this starting point, a wide variety of mathematical operations can be applied on a case-by-case basis. For example, exact solutions can be developed into the form of differential equations, such as the case in Tutuncu & Ozturk (2001). However, differential equations are not ideal because they are slow to solve. To improve on this, numerical methods were usually employed to greatly reduce the computing time.

For instance, in the case of a spherical pressure vessel in Kalanta et al. (2013), Castigliano's principle is applied, and the equations are arranged into matrix form to form a convex nonlinear programming problem. The Bubnov-Galerkin method is referenced to replace the model's differential equations with algebraic equations.

Tutuncu & Temel (2009) offers an interesting take on developing the exact solution for FGM spheres, along with disks and cylinders as well. The Complementary Functions Method (CFM) was implemented in the solution, reducing the boundary value problem into an initial value problem, which can then be easily resolved with the aid of numerical methods such as the Runge-Kutta method. With this approach, the resulting numerical results is accurate up to the sixth digit using only Runge-Kutta method of fifth order, also known as RK5.

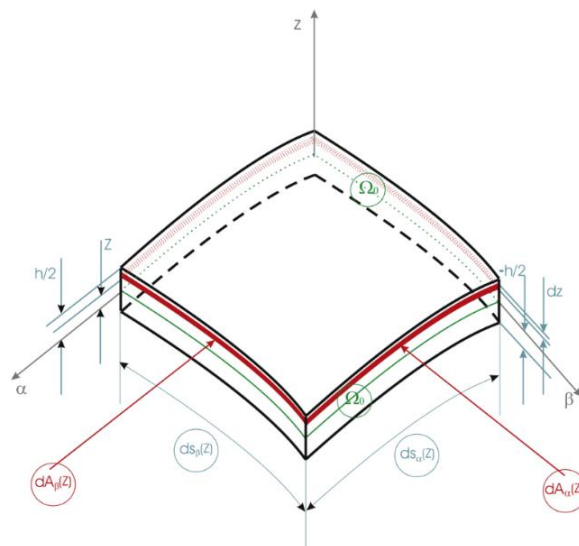
Other studies that have also applied numerical methods in their solutions are Bayat et al. (2011) and Fukui & Yamanaka (1992). Bayat has proposed to

assign an arbitrary value to a dimensionless parameter, β , which affects the stresses in a spherical vessel. By manipulating the value of β , the FGM vessel can indeed be tailored to ensure the lowest stress levels are reached. The results from this study agrees with both simulations and existing data, with a maximum percentage error of 1.12%. This error is attributed to the assumption that the modulus of elasticity in each layer is constant throughout the structure. The conclusion drawn from this paper coincides with another paper published by Chen & Lin (2008), where the parameter β was observed to affect the stress distribution along the radial direction of a spherical vessel by a significant margin.

There are also a number of creative approaches to this problem. Brischetto (2017) has proposed an interesting way to develop an exact solution that can be applied to plates, shells, spheres as well as cylinders. As shown in Figure 2.2(a) below, the idea is to develop the model initially as a three-dimensional shell, with a curvilinear orthogonal reference system (α , β and z axes).

Using this base model, the shell can be modelled as any other shape with some slight modifications to the equations, as seen in Figure 2.2(b). This is done with clever manipulation of the reference system.

(a)



(b)

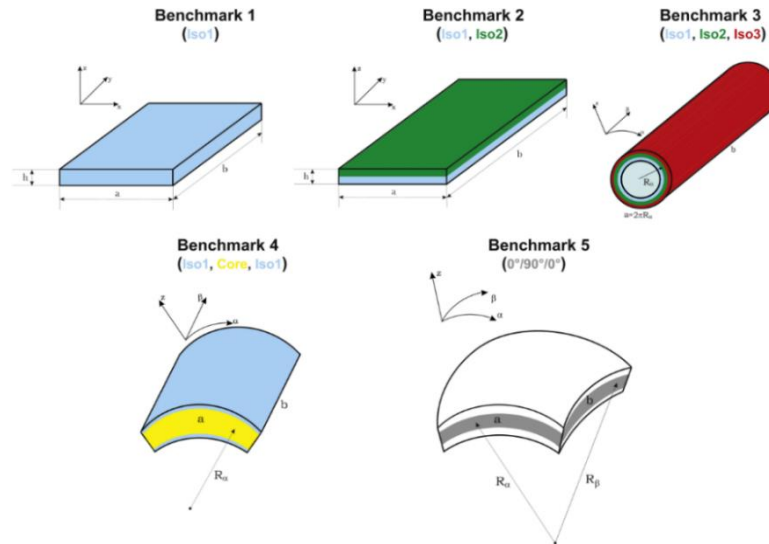


Figure 2.2: (a) the Geometrical Data and Notations for a 3D Shell Model, and (b) Different Geometries Achievable via Modifying the Reference System (Brischetto, 2017).

2.5 Finite Element Analyses of Pressure Vessels

According to Zienkiewicz et al. (2005), the basis of FEA is to approximate the behaviour of a continuum by the “finite elements”. These elements behave similarly to the “real elements” in actual structures. These “real” elements are known as discrete elements.

When put under FEA, a structure would be modelled as a discrete model with a finite number of degrees of freedom (Kalanta, et al., 2013). The structure gets broken down into countless small chunks, as shown in Figure 2.3 below. Each of these elements will be examined individually during the simulation.

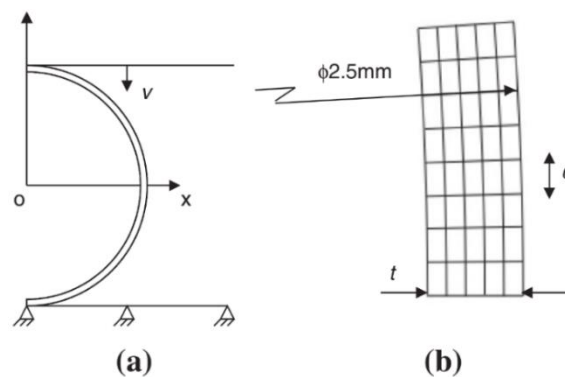


Figure 2.3: (a) A Single-layered Hollow Sphere in Axisymmetric Configuration, and (b) A Zoomed-in View of the Model (Li, et al., 2012).

In general, the accuracy of the solution increases as the mesh size decreases. However, not all projects can afford to run the simulation at the smallest possible mesh size, simply because of constraints in computing power and time. As seen in Figure 2.4(b), in cases where the mesh sizing must be reduced to reduce the computational load, the edges of each of the layers should be refined. This is to compensate for the possibility of a stress discontinuity at the interface between layers, where material properties shift abruptly. The continuous areas in the middle of the layers, on the other hand, can be left with a coarser mesh (Somadder & Islam, 2015).

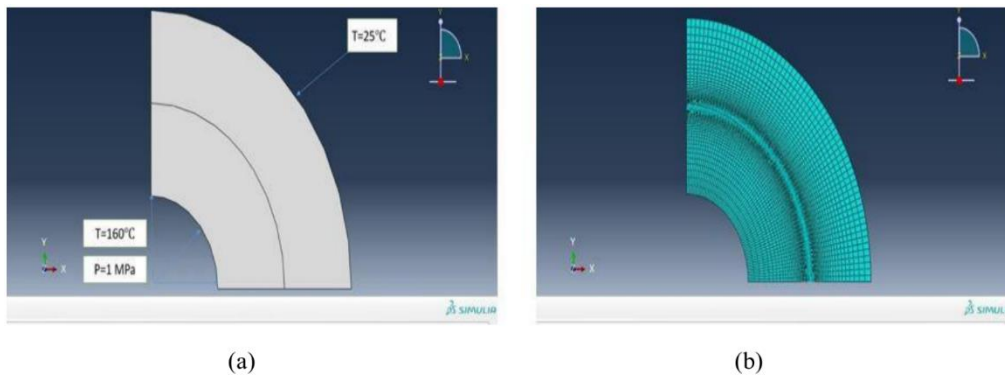


Figure 2.4: (a) A 2D FEA Model, and (b) Demonstration of Meshing Priorities (Somadder & Islam, 2015).

Other than that, it is also common practice not to model for the entire structure while performing FEA. Referring to Figure 2.4(a) again, only one-fourth of the model was used in this 2D analysis. This can only be used when both the geometry as well as boundary conditions are symmetric on all sides. When these requirements are fulfilled, using this method would save precious computing time.

The solution from a Finite Element Analysis serves as a basis to verify results from other sources. Zhang et al. (2012) has produced an analytical solution with results that coincide perfectly with the set of results obtained from ANSYS. A comparison is provided in the Figure 2.5 below.

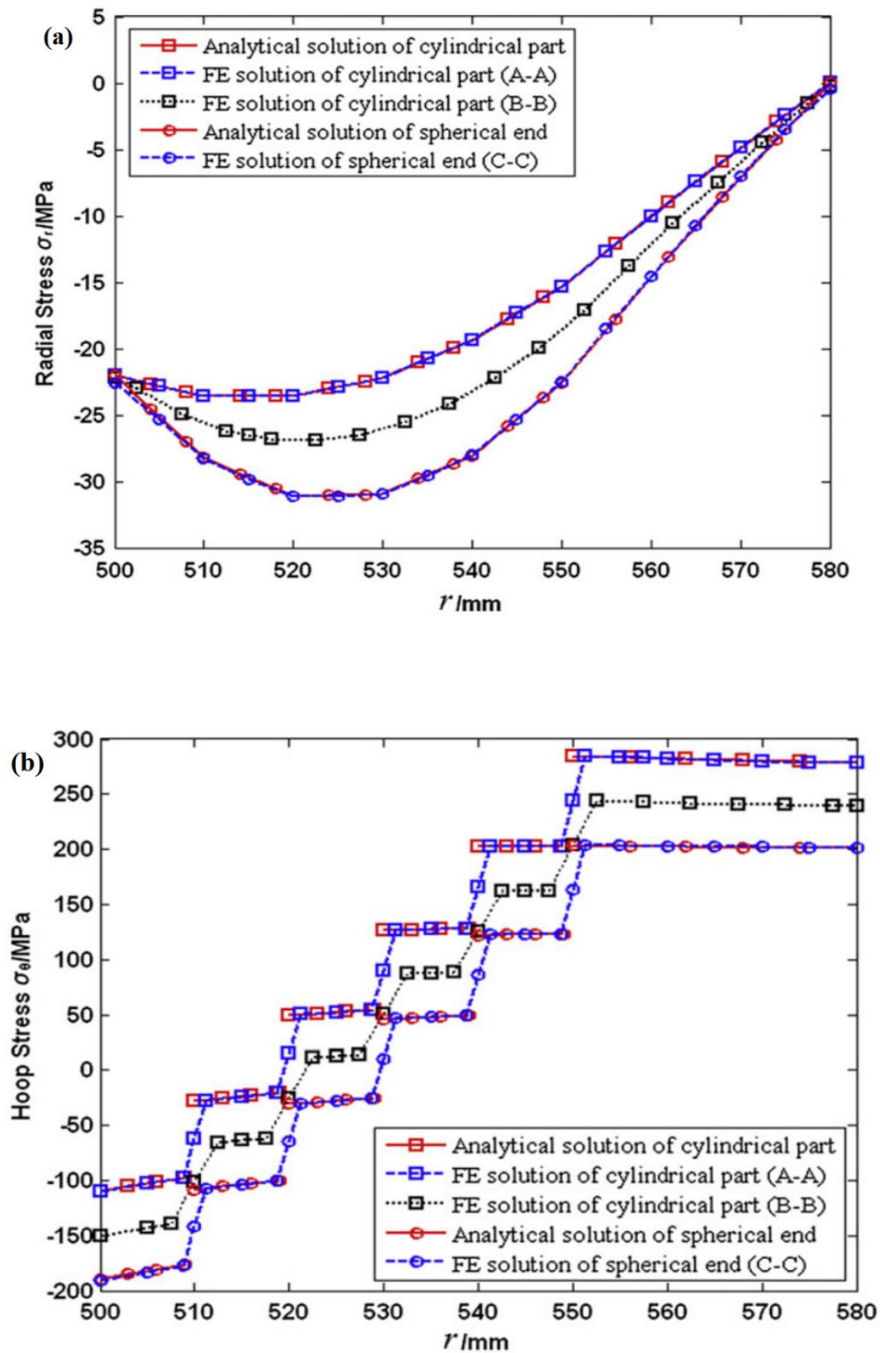


Figure 2.5: Comparison between the Analytical Solution and the FEA Solution for the (a) Radial Stress, and (b) Hoop Stress (Zhang, et al., 2012).

2.6 Summary

From the papers focusing on the mathematical solutions for the mechanical stresses in multilayered spherical vessels, Tutuncu & Ozturk (2001) has proposed an exact solution via differential equations. Kalanta et al. (2013) has applied Castigliano's principle and replaced the differential equations with algebraic equations via the Bubnov-Galerkin method. Other numerical methods were used by Tutuncu & Temel (2009), Bayat et al. (2011), and Fukui & Yamanaka (1992) to arrive at their respective final results.

To conclude the literature review, even though many hours of research have been dedicated to this field, there is still a slight gap whereby there is no analytical solution proposed specifically to model for the stress distribution for multilayered spherical pressure vessels. Instead of solving for the differential equations directly, a recurrence relation equation would be introduced via the recursive method to solve for the final outcome. This solution does not require the use of numerical methods, and is capable of producing quick and accurate outcome.

CHAPTER 3

METHODOLOGY AND WORK PLAN

3.1 Introduction

For the purpose of this project, both analytical solution and simulation of the mechanical stress distribution will be completed. However, both of these solutions provide only theoretical results. They have to be verified whether or not its authenticity can be translated into real life situations. Without a proper verification of the accuracy of the solution, this project cannot be considered a success. Therefore, a set of results is to be retrieved from published papers from reliable sources to act as a reference. This will give us three sources of results in total. These independent sets of results will then be compared to verify the accuracy of the proposed solution.

3.2 Development of the Solution

The development of this analytical solution was largely adapted from the paper published by Yeo et al. (2017). Starting from the stress-strain relation equations and the strain-displacement equations in Equation 2.1 and Equation 2.2, an analytical solution was developed via the recursive method. This solution can then be programmed in MATLAB to retrieve the final values of the stresses and displacement.

According to Hetnarski & Eslami (2009), for the inner surface, the radial boundary conditions of the sphere are

$$\sigma_{rr,1}(r_0) = -q_0 = -P_{int} \quad (3.1)$$

where P_{int} is the pressure exerted on the inner surface, and $\sigma_{rr,1}(r_0)$ denote the radial stress exerted on the inner surface of the first layer.

For the outer surface, the boundary conditions are

$$\sigma_{rr,n}(r_n) = -q_n = -P_{ext} \quad (3.2)$$

where P_{ext} is the pressure exerted on the outer surface, and $\sigma_{rr,n}(r_n)$ denote the radial stress on the outer surface of the n -th layer.

For each interface between the layers i and $i + 1$, the displacement and the radial stress are

$$\sigma_{rr,i}(r) = \sigma_{rr,i+1}(r) \quad (3.3a)$$

$$u_{r,i}(r) = u_{r,i+1}(r) \quad (3.3b)$$

Stress-strain relations for spherical structures for the i -th layer is commonly known as

$$\varepsilon_{rr,i} = \frac{1}{E_i} [\sigma_{rr,i} - 2\nu\sigma_{\phi\phi,i}] \quad (3.4a)$$

$$\varepsilon_{\phi\phi,i} = \frac{1}{E_i} [(1 - \nu)\sigma_{\phi\phi,i} - \nu\sigma_{rr,i}] \quad (3.4b)$$

Next, the strain-displacement relation is

$$\varepsilon_{rr,i} = \frac{d}{dr}(u_r) \quad (3.5a)$$

$$\varepsilon_{\phi\phi,i} = \frac{u_r}{r} \quad (3.5b)$$

The equilibrium equation for a sphere can be expressed as

$$\frac{d}{dr}(\sigma_{rr,i}) + \frac{2(\sigma_{rr,i} - \sigma_{\phi\phi,i})}{r} \quad (3.6)$$

Substituting (3.5) into (3.4) and then into (3.6) yields

$$\frac{d}{dr} \left[\frac{1}{r^2} \frac{d}{dr} (u_r r^2) \right] = 0 \quad (3.7)$$

Integrating (3.7) returns

$$u_{r,i}(r) = C_i r + \frac{D_i}{r^2} \quad (3.8)$$

From the strain-displacement relation in (3.5),

$$\varepsilon_{rr,i} = \frac{d}{dr} [u_{r,i}(r)] = C_i - \frac{2D_i}{r^3} \quad (3.9a)$$

$$\varepsilon_{\phi\phi,i} = \frac{u_{r,i}(r)}{r} = C_i + \frac{D_i}{r^3} \quad (3.9b)$$

Substituting (3.8) into (3.5) and (3.4) gives

$$\sigma_{rr,i}(r) = \frac{E_i}{(1-2\nu)} C_i - \frac{2E_i}{(1+\nu)r^3} D_i \quad (3.10a)$$

$$\sigma_{\phi\phi,i}(r) = \frac{E_i}{(1-2\nu)} C_i + \frac{E_i}{(1+\nu)r^3} D_i \quad (3.10b)$$

Let

$$\beta_i = \frac{(1-2\nu)}{E_i} \text{ and } \lambda_i = \frac{-(1+\nu)}{2E_i}$$

Equation (3.10) becomes

$$\sigma_{rr,i} = \frac{C_i}{\beta_i} + \frac{D_i}{\lambda_i r^3} \quad (3.11a)$$

$$\sigma_{\phi\phi,i} = \frac{C_i}{\beta_i} - \frac{D_i}{2\lambda_i r^3} \quad (3.11b)$$

To further simplify this, let

$$\hat{C}_i = \frac{C_i}{\beta_i} \text{ and } \hat{D}_i = \frac{D_i}{\lambda_i}$$

Equation (3.11) and (3.8) becomes

$$\sigma_{rr,i}(r) = \hat{C}_i + \frac{\hat{D}_i}{r^3} \quad (3.12a)$$

$$\sigma_{\phi\phi,i}(r) = \hat{C}_i - \frac{\hat{D}_i}{2r^3} \quad (3.12b)$$

$$u_{r,i}(r) = \beta_i \hat{C}_i r + \lambda_i \frac{\hat{D}_i}{r^2} \quad (3.12c)$$

The constants \hat{C}_i and \hat{D}_i is to be determined using equations (3.3a) and (3.3b). This will be useful in determining both the radial stresses as well as the displacements across the wall of the sphere. The outcome is

$$\hat{C}_i + \frac{\hat{D}_i}{r_i^3} = \hat{C}_{i+1} + \frac{\hat{D}_{i+1}}{r_i^3} \quad (3.13a)$$

$$\beta_i \hat{C}_i r_i + \lambda_i \frac{\hat{D}_i}{r_i^2} = \beta_{i+1} \hat{C}_{i+1} r_i + \lambda_{i+1} \frac{\hat{D}_{i+1}}{r_i^2} \quad (3.13b)$$

By solving equations (3.13a) and (3.13b), \hat{C}_{i+1} and \hat{D}_{i+1} are expressed as

$$\hat{C}_{i+1} = \hat{C}_i \left[\frac{\lambda_{i+1} - \beta_i}{\lambda_{i+1} - \beta_{i+1}} \right] + \frac{\hat{D}_i}{r_i^3} \left[\frac{\lambda_{i+1} - \lambda_i}{\lambda_{i+1} - \beta_{i+1}} \right] \quad (3.14a)$$

$$\hat{D}_{i+1} = \hat{C}_i r_i^3 \left[\frac{\beta_i - \beta_{i+1}}{\lambda_{i+1} - \beta_{i+1}} \right] + \hat{D}_i \left[\frac{\lambda_i - \beta_{i+1}}{\lambda_{i+1} - \beta_{i+1}} \right] \quad (3.14b)$$

For two adjacent layers, their radial stresses can be expressed as

$$\sigma_{rr,i}(r_{i-1}) = -q_{i-1} \quad (3.15a)$$

$$\sigma_{rr,i+1}(r_{i+1}) = -q_{i+1} \quad (3.15b)$$

The corresponding contact pressure is

$$\hat{C}_i + \frac{\hat{D}_i}{r_{i-1}^3} = -q_{i-1} \quad (3.16a)$$

$$\hat{C}_{i+1} + \frac{\hat{D}_{i+1}}{r_{i+1}^3} = -q_{i+1} \quad (3.16b)$$

Substituting (3.16) into (3.14) gives

$$\hat{C}_i = \frac{q_{i+1}(\lambda_{i+1} - \beta_{i+1}) - q_{i-1}S_i}{S_i - G_i} \quad (3.17a)$$

$$\hat{D}_i = \gamma_i r_i^3 \left[\frac{-q_{i+1}(\lambda_{i+1} - \beta_{i+1}) + q_{i-1}G_i}{S_i - G_i} \right] \quad (3.17b)$$

where

$$S_i = \gamma_i \gamma_{i+1} (\lambda_i - \beta_{i+1}) + \gamma_i (\lambda_{i+1} - \lambda_i) \quad (3.18a)$$

$$G_i = (\lambda_{i+1} - \beta_i) + \gamma_{i+1} (\beta_i - \beta_{i+1}) \quad (3.18b)$$

$$\gamma_{i+1} = \frac{r_i^3}{r_{i+1}^3} \quad (3.18c)$$

On the outer surface of the i -th layer, the radial stress and the contact pressure is related in the form of

$$\sigma_{rr,i}(r_i) = -q_i \quad (3.19)$$

Equation (3.19) can be expressed as the following via substituting (3.12a)

$$\hat{C}_i + \frac{\hat{D}_i}{r_i^3} = -q_i \quad (3.20)$$

Substituting (3.17) into (3.20)

$$q_{i+1} = \frac{-q_i(S_i - G_i) + q_{i-1}(S_i - \gamma_i G_i)}{(1 - \gamma_i)(\lambda_{i+1} - \beta_{i+1})} \quad (3.21)$$

Substituting (3.21) into (3.17) yields

$$\hat{C}_i = \frac{q_{i-1}\gamma_i - q_i}{1 - \gamma_i} \quad (3.22a)$$

$$\hat{D}_i = \gamma_i r_i^3 \left[\frac{-q_{i-1} + q_i}{1 - \gamma_i} \right] \quad (3.22b)$$

To solve \hat{C}_i and \hat{D}_i and subsequently define q_i in terms of q_0 and q_n , two recurrence relations is expressed with respect to (3.21) as

$$c_{i+1} = \frac{-c_i(S_i - G_i) + c_{i-1}(S_i - \gamma_i G_i)}{(1 - \gamma_i)(\lambda_{i+1} - \beta_{i+1})} \quad (3.23a)$$

$$d_{i+1} = \frac{-d_i(S_i - G_i) + d_{i-1}(S_i - \gamma_i G_i)}{(1 - \gamma_i)(\lambda_{i+1} - \beta_{i+1})} \quad (3.23b)$$

where $i = 1, 2, \dots, (n - 1)$.

Introducing q_i in terms of the recurrence relations result in

$$q_i = c_i q_1 + d_i q_0 \quad (3.24)$$

Where the initial values are given as

$$c_0 = 0, \quad c_1 = 1, \quad d_0 = 1, \quad d_1 = 0$$

When $i = n$, it is found that

$$q_1 = \frac{q_n - d_n q_0}{c_n} \quad (3.25)$$

Therefore, solving q_i with respect to the recurrence relations as well as its boundary values will give

$$q_i = \frac{c_i}{c_n} P_{ext} + \left(d_i - \frac{d_n}{c_n} c_i \right) P_{int} \quad (3.26)$$

3.3 Computational Procedures for the Solution

The coding in MATLAB is programmed according to the following steps:

1. Determine the sequences of S_i , G_i , and γ_i in equation (3.18).
2. Find the sequences of c_i and d_i in equation (3.23), followed by computing the sequences of q_i in (3.26) using the values of c_i and d_i .
3. Compute the sequences of \hat{C}_i and \hat{D}_i in (3.22).
4. Finally, the radial displacement in (3.12c) and stresses in equations (3.12a) and (3.12b) can be determined with the use of sequences \hat{C}_i and \hat{D}_i .

3.4 Geometry, Material Properties, and Boundary Conditions

The paper chosen to serve as a reference was written by Bayat et al. (2011). The model used in this paper is a spherical vessel made of functionally graded materials, whereby the elastic modulus was defined by the following function:

$$E(r) = E_i r^\beta \quad (3.27)$$

where $E_i = 200 \text{ GPa}$.

The symbol β refers to the inhomogeneity factor. This factor determines the type of distribution of one of the constituents within the structure. For example, an FGM plate with an inhomogeneity factor of 1 will have a linearly increasing concentration of a particular constituent along the thickness direction. For the sake of simplicity, the inhomogeneity factor used was $\beta = 1$. Therefore, the actual elastic modulus distribution can be simplified as:

$$E(r) = E_i r \quad (3.28)$$

where $E_i = 200 \text{ GPa}$.

Apart from the elastic modulus, the Poisson's ratio of the material was set at a constant $\nu = 0.3$ throughout the structure.

The boundary condition configured is the internal pressure with a magnitude of 80 MPa, with no external pressure. The material properties and boundary conditions of this model will be applied in both the proposed analytical solution as well as the finite element analysis. This is to ensure the comparability of the results across all three sources. The results from the graphs included in this paper were extracted from the graphs via DigXY for the comparisons.

A Finite Element Analysis of a simple multilayered pressure vessel will be done next. ANSYS Mechanical is a very useful tool to model for these simple structures. In the case of a sphere, only a quarter of a sphere has to be modelled manually. This results in a semi-hemisphere. From there, the mechanical properties of each layer within the vessel can be defined accordingly. The

boundary conditions and initial conditions are to be properly set up in this phase as well.

Ideally, the FEA would be modelled as an FGM sphere to better match the reference model. Unfortunately, FEA software solutions currently available on the market do not support the application of FGMs. The best alternative is to divide the model into as many layers as possible. Thus, a 20 layered model was simulated to replace an FGM vessel.

By configuring for 2D axisymmetric analysis, followed by a displacement constraint placed at one edge of the model, this semi-hemisphere can be mirrored into a proper spherical structure. A rough sketch of the model is included in Figure 3.1. This model will be solved for its Total Deformation, Maximum Principal Stress, Middle Principal Stress, and Minimum Principal Stress.

The rest of the analysis is up to the software to operate by itself. The simulation will iterate over and over again until the difference in the results produced from two consecutive runs is lower than the predefined value. At that point, the final outcome is to be retrieved and is ready for further use.

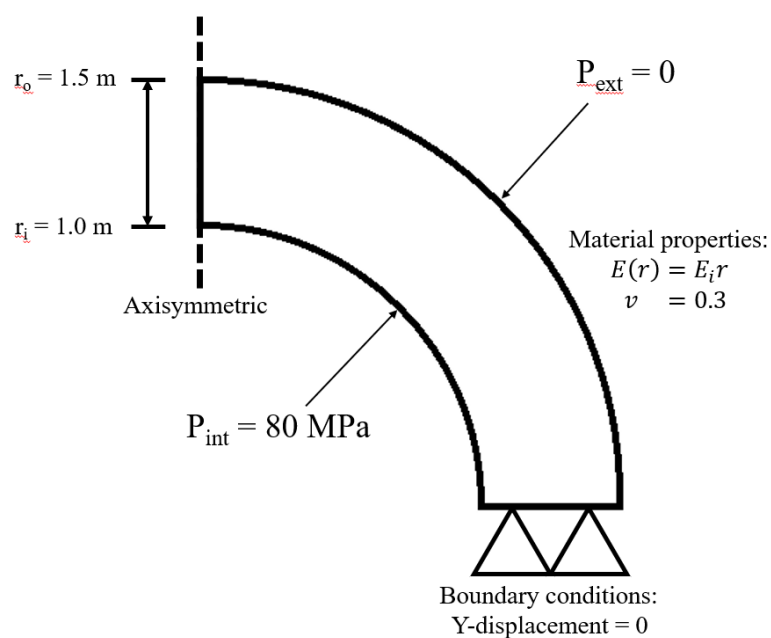


Figure 3.1: A Sketch of the 2D FEA Model.

Referring to Figure 3.1, the boundary conditions are only defined on one of the two flat edges of the model. This is because the geometry of the model was set to be axisymmetric, and therefore, the model will be revolved around the vertical flat edge to form a complete structure.

As mentioned above, modelling for the entire sphere in 3D space is not necessary in this project, because this model is an axisymmetric structure without irregularities in the geometry. A 2D analysis of a quarter of a sphere will be sufficient for the purposes of this project. The geometry of the structure will be modelled using DesignModeler, while the analysis itself will be run in ANSYS Mechanical. The step-by-step procedures of this operation is detailed below.

3.4.1 Initializing

1. ANSYS Workbench was launched, and the project was saved with an appropriate file name.
2. From the toolbox on the left, “Static Structural” was selected by double-clicking.
3. The “Properties of Schematic” pane on the right of the window was accessed by single-clicking on “Geometry”. Under “Advanced Geometry Options”, 2D Analysis was selected for the “Analysis Type” option.

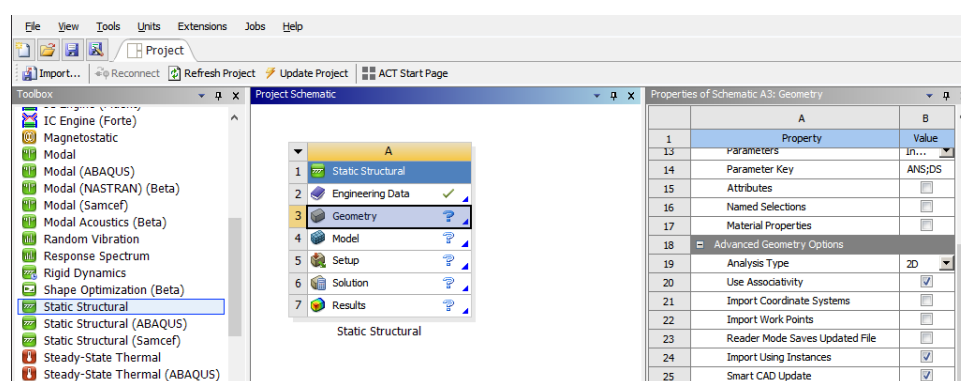


Figure 3.2: The Main Window.

4. To configure the materials to be used in the simulation, “Engineering Data” was accessed with a double-click, followed by opening the “A2: Engineering Data” tab. Clicking on “General Materials” gives a list of materials commonly used. Custom materials can also be defined with custom mechanical properties here. Clicking on the ‘+’ button adds the particular material into the shortlist of materials available in the later parts of the simulation.

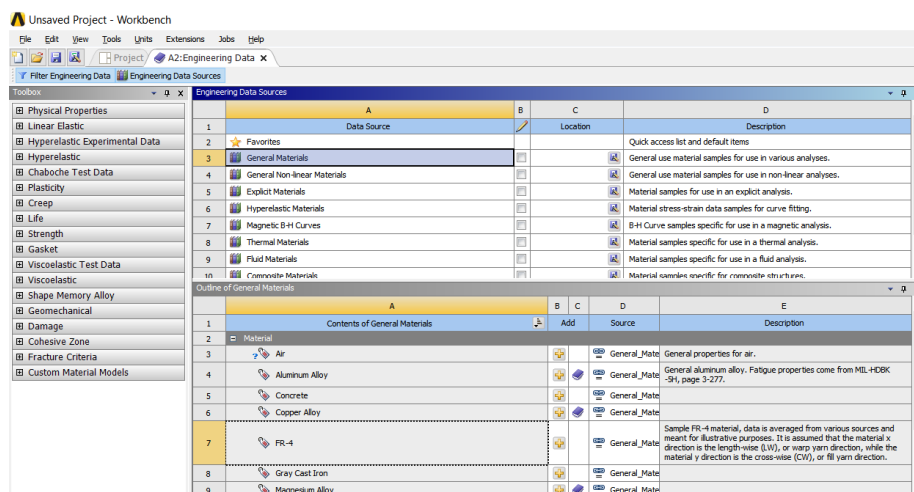


Figure 3.3: The Engineering Data Page.

5. If a custom material is needed, “Create Custom Model” can be selected under “Custom Material Models”. The material properties can be defined manually by selecting on the proper category on the left pane.

3.4.2 Geometry

1. The “Geometry” selection was right-click and the DesignModeler program was launched. Alternatively, double-clicking on “Geometry” launches the SpaceClaim program instead. Both options are capable of developing a 3D model of the desired structure.

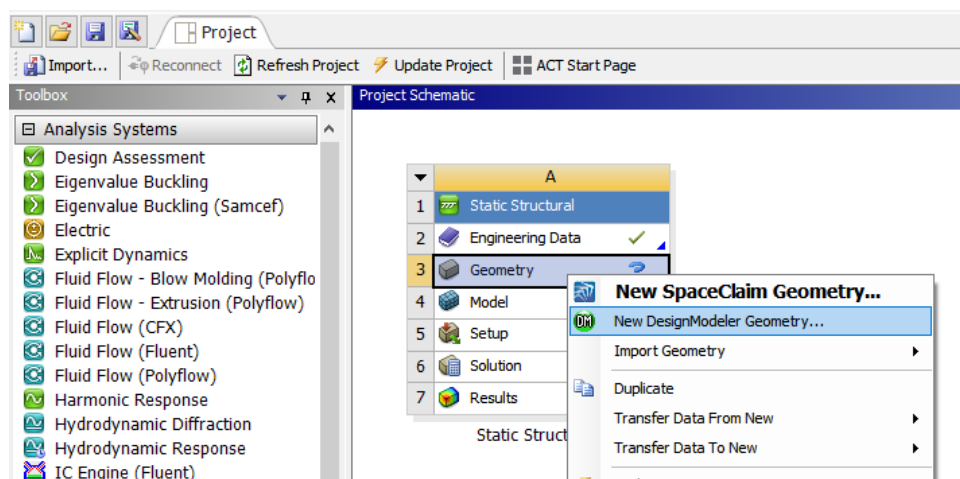


Figure 3.4: Creating a New Geometry via DesignModeler.

2. In DesignModeler, the model will be sketched on the XY Plane, since ANSYS Mechanical defines the Y-axis as the revolving axis for axisymmetric applications. This is done by clicking on “Look at Face” after selecting the XY lane.

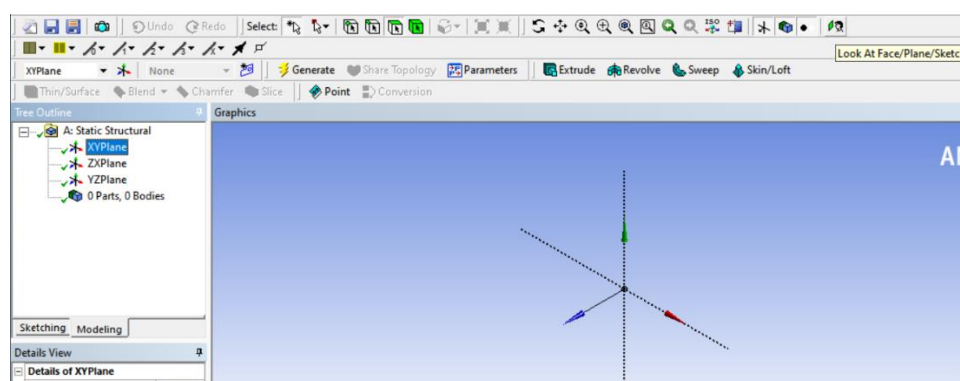


Figure 3.5: Selecting “Look At Face” at the Upper Right Corner.

- Using the “Arc from Center” and “Line” functions, the following sketch was made in DesignModeler without precise dimensions. These two arcs will be modelled as the innermost and outermost layers of the pressure vessel. The radii of the two arcs were defined after the sketch was complete as 0.3m and 0.36m, respectively.

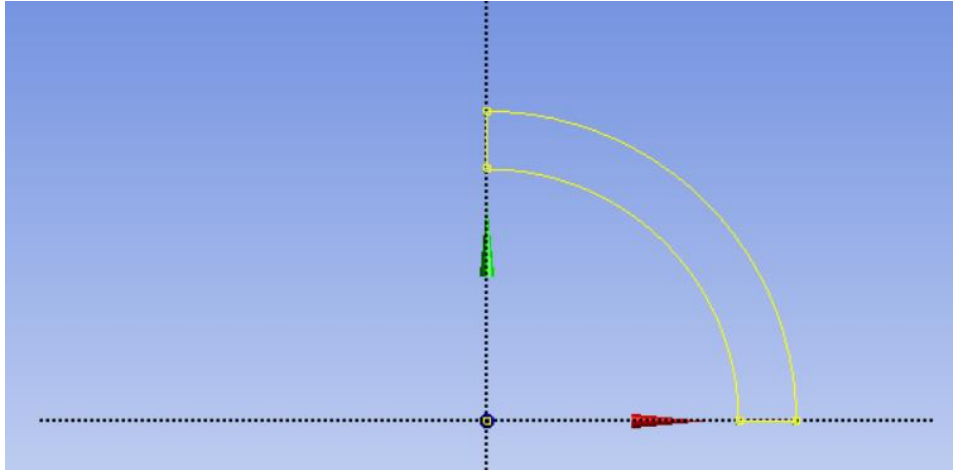


Figure 3.6: Outlining a Semi-hemisphere.

- The area enclosed within the two arcs were then modelled as a surface by running the “Surfaces From Sketches” function under the “Concepts” tab.

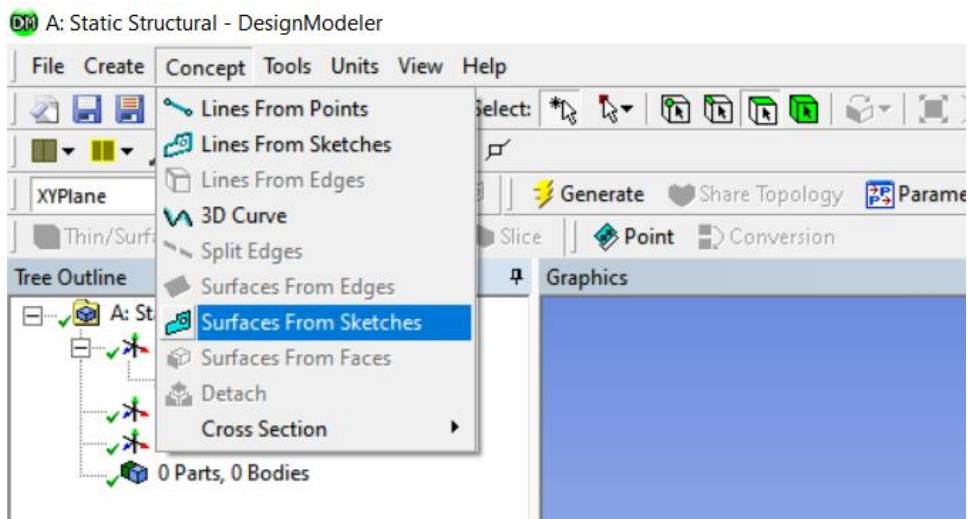


Figure 3.7: Generating a Body from the Sketch.

5. Next, a new plane was created. More arcs were sketched as the boundaries between adjacent layers within the pressure vessel. The number of arcs depend on the number of layers selected for the model. Since this is a 20 layered model, 19 more arcs were sketched.

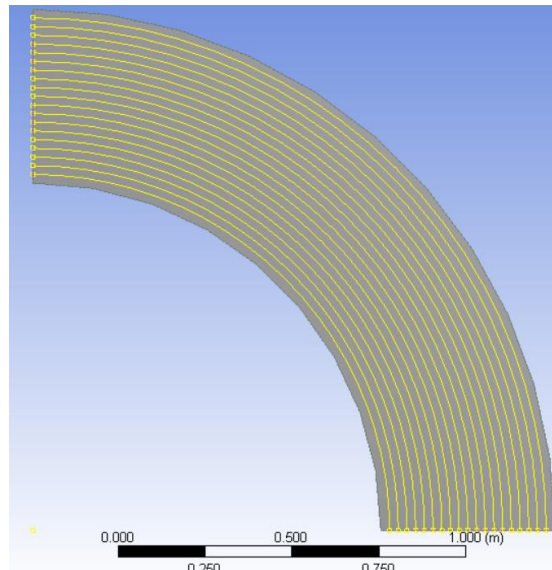


Figure 3.8: Creating a New Sketch to Sketch the Layer Interfaces.

6. This time, instead of generating a surface from the sketch, the “Extrude” function is used instead. The configuration for this operation is set to “Slice Material” instead of the default “Add Material”.

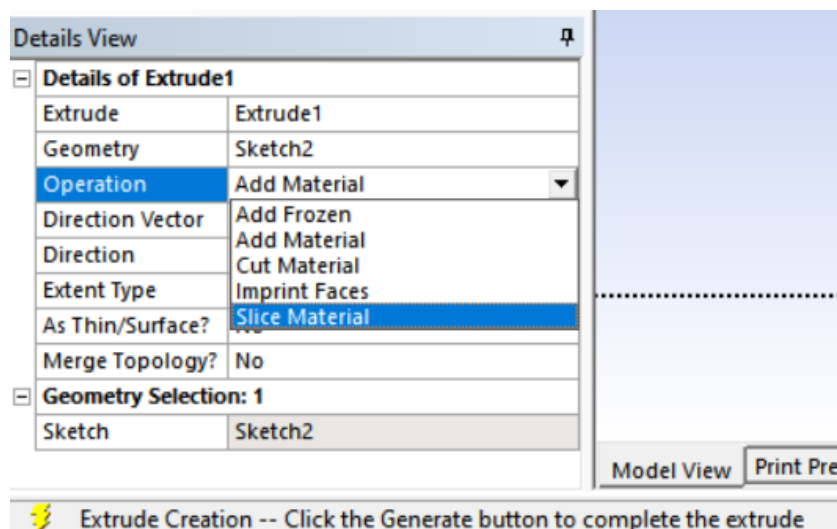


Figure 3.9: Selecting “Slice Material” to Cut the Body into Different Layers.

7. The resulting model was made sure to consist of six separate bodies, one for each layer. The project was then saved to move on to the next part.

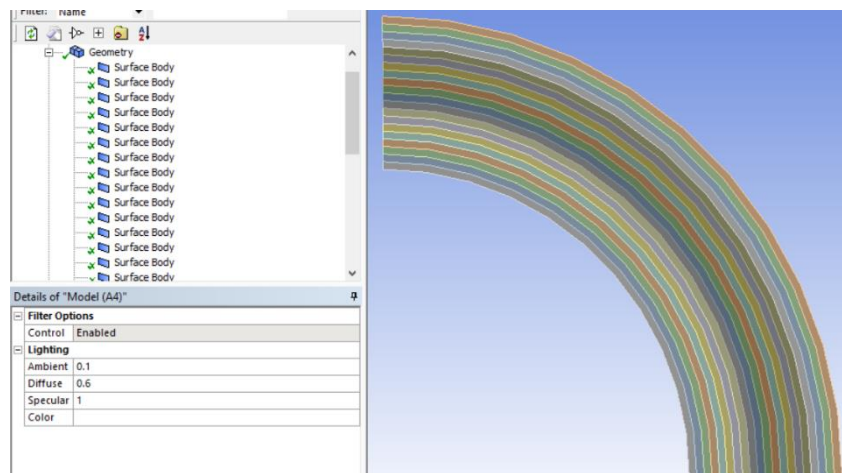


Figure 3.10: The Finalized Sketch of a Multilayered Sphere.

3.4.3 Model

1. ANSYS Mechanical was launched by double-clicking on “Model” on the workbench.
2. The very first thing to do in Mechanical was to configure the “2D Behavior” under “Geometry” to “Axisymmetric”.

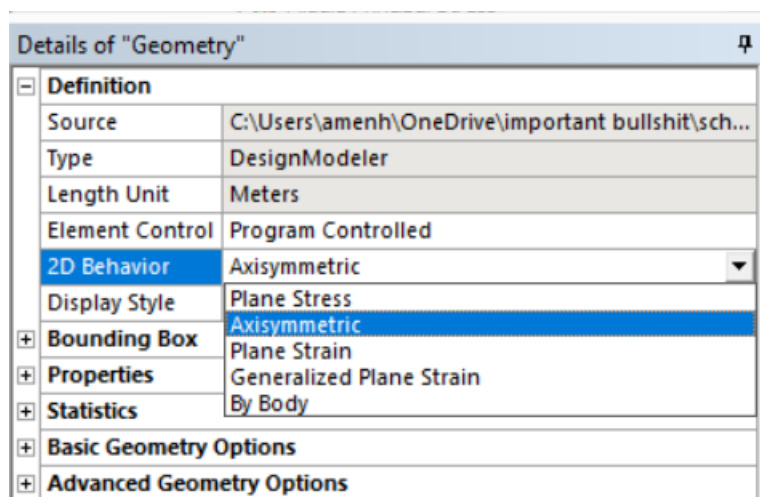


Figure 3.11: Configuring the System as Axisymmetric.

3. On the left panel, “Model” was right-clicked to insert a “Construction Geometry”.

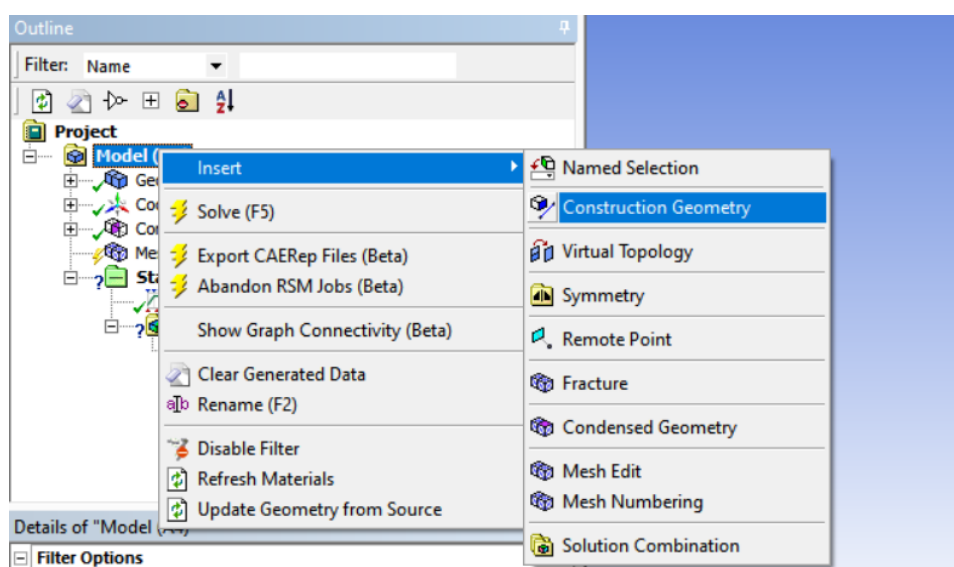


Figure 3.12: Setting Up a Construction Geometry.

- Following up from the previous step, “Construction Geometry” was right-clicked to insert a “Path”.

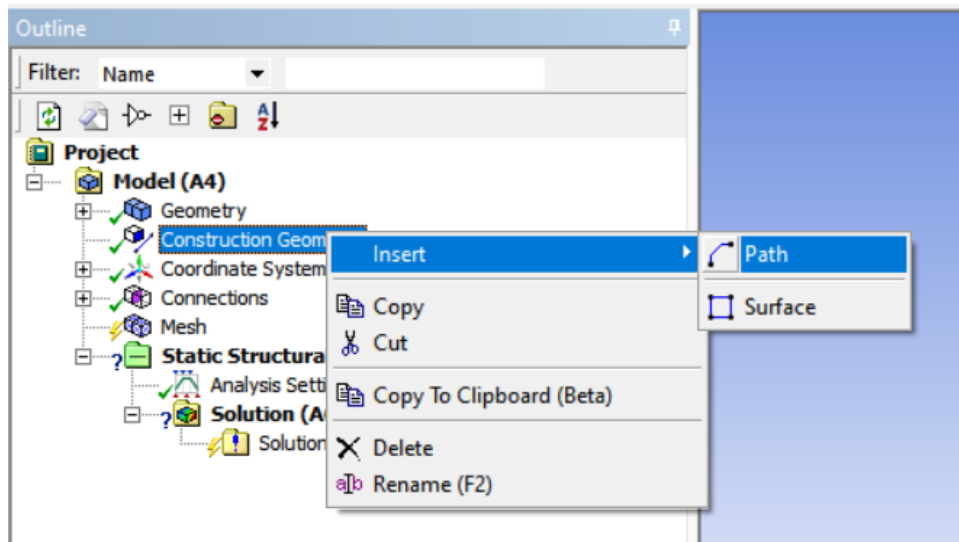


Figure 3.13: Inserting a Path.

- This path was defined along the radial direction at the bottom part of the model. For the purpose of this simulation, this path can be defined at any point on the model, as long as it passes through the origin of the sketch.

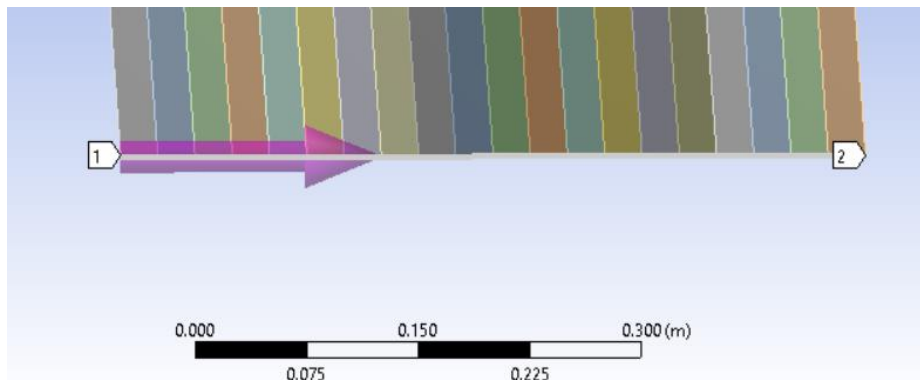


Figure 3.14: Defining the Path.

6. Next, the mesh sizing was defined under “Mesh Control”.

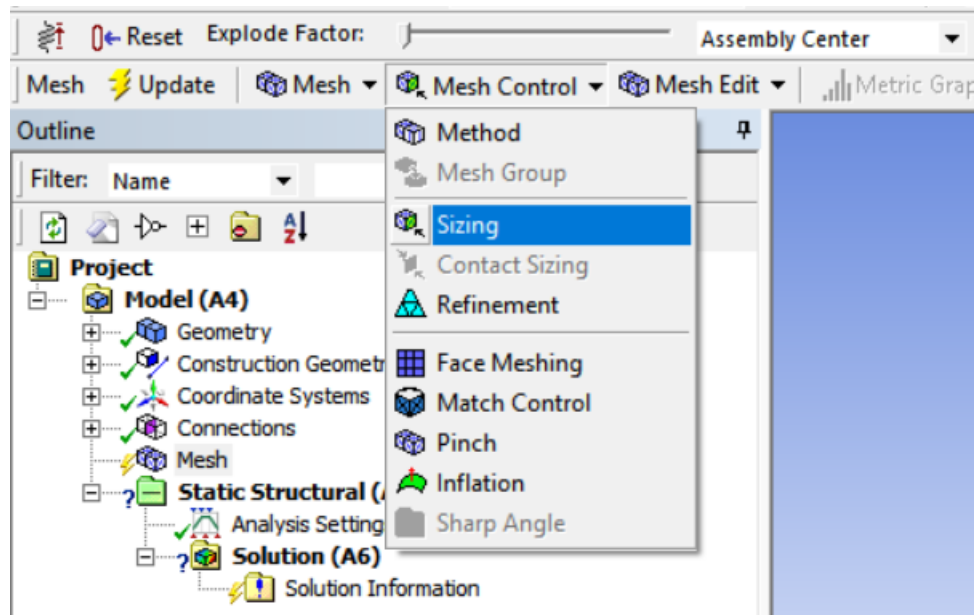


Figure 3.15: Constraining the Mesh by its Sizing.

7. The minimum element size was defined as 0.0025m. The mesh was generated by clicking on “Update”.

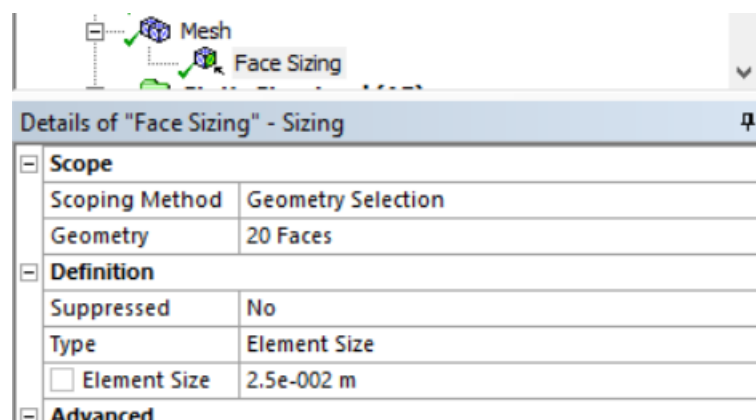


Figure 3.16: Generating the Mesh with a Predefined Element Size.

8. To define the loading condition of the model, “Pressure” was selected under “Loads”.

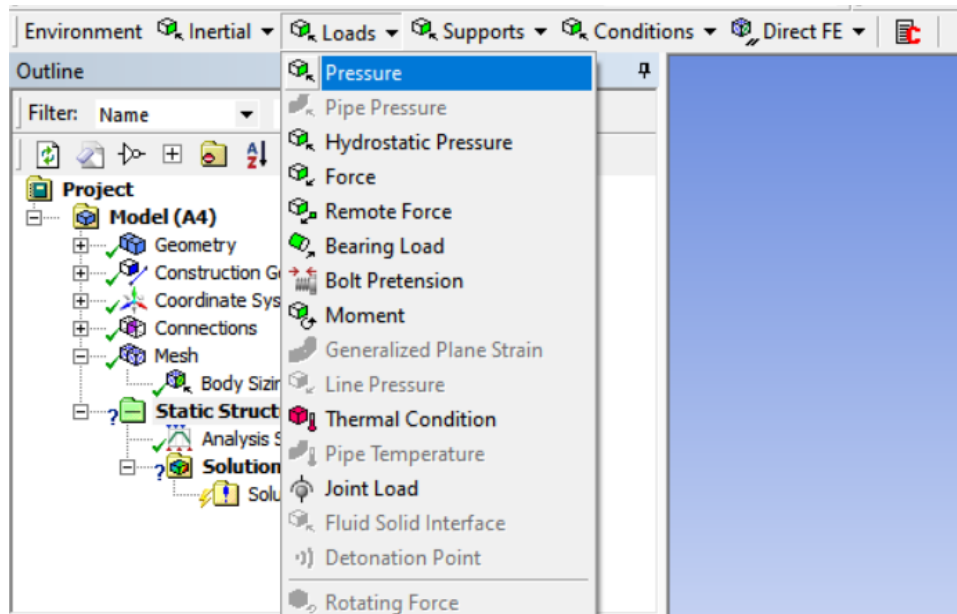


Figure 3.17: Defining the Loading Conditions.

9. The innermost surface of the model was selected and an internal loading pressure of 80 MPa was applied. The same was done to the outer surface with an external loading equivalent to the atmospheric pressure.

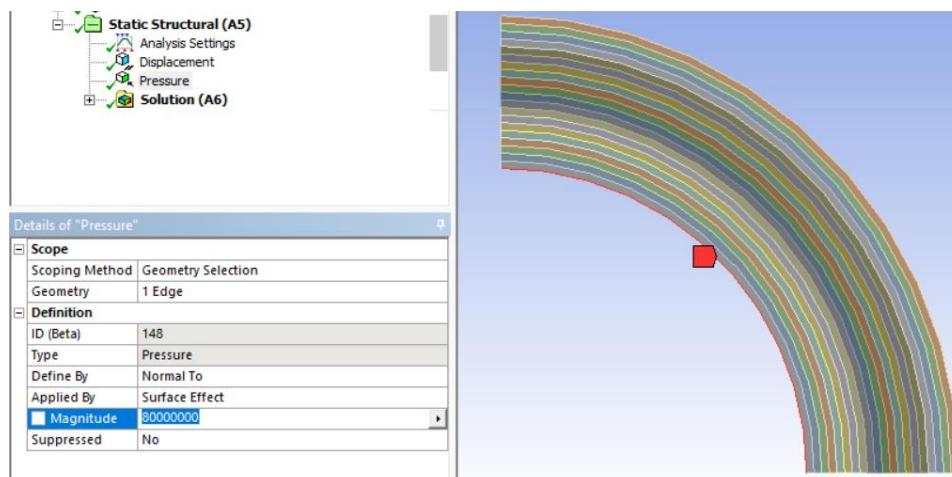


Figure 3.18: Defining the Inner and Outer Pressures.

10. A constraint was placed at the bottom part of the model to allow no deformations in the Y-direction. This was accomplished by selecting “Displacement” under “Supports”.
11. All six edges were selected and given a “0” value for the Y-component.

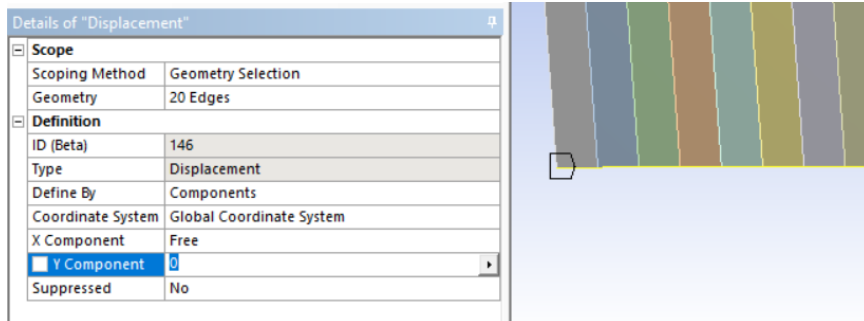


Figure 3.19: Constraining the Displacement in the Y-direction.

3.4.4 Execution and Data Retrieval

1. “Total” was selected under the “Deformation” tab, which represents the radial displacement of the structure.
2. Under the “Scoping Method”, “Path” was chosen to exclusively retrieve the data along the path designated earlier.

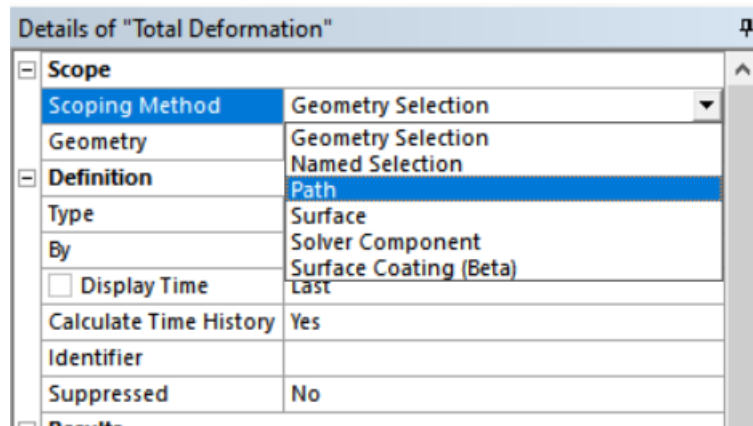


Figure 3.20: Confining the Simulation on the Path Created.

3. Other solutions were also added, including the maximum principal stress, middle principal stress, and the minimum principal stress. Similar to the above step, these solutions were also configured to “Scoping Method = Path”.
4. The simulation was executed by clicking “Solve” on the toolbar above.
5. After the computation has completed, the data was retrieved by right-clicking on the solution and running the “Export Text File” command.

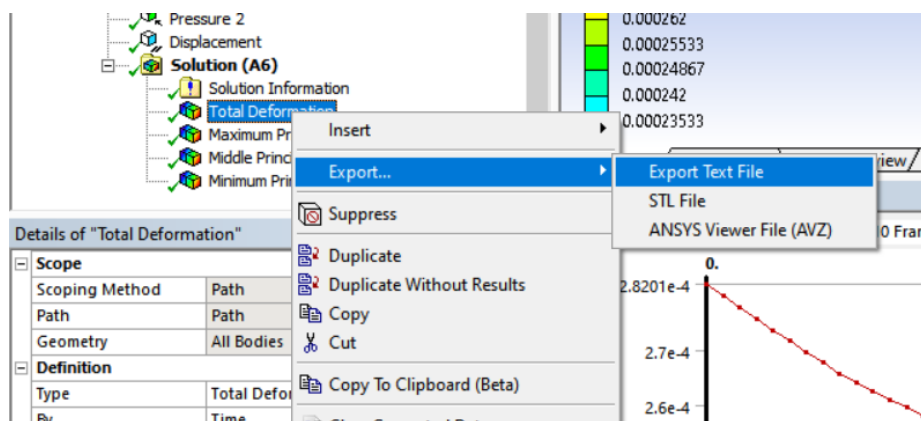


Figure 3.21: Exporting the Data.

6. The data was then opened as an Excel file for further data manipulation.

	A	B	C	D	E	F
1	S (m)	X Coordinate (m)	Y Coordinate (m)	Z Coordinate (m)	Total Deformation (m)	
2	0	0.3	0	0	2.82E-04	
3	1.25E-03	0.30125	0	0	2.80E-04	
4	2.50E-03	0.3025	0	0	2.78E-04	
5	3.75E-03	0.30375	0	0	2.76E-04	
6	5.00E-03	0.305	0	0	2.74E-04	
7	6.25E-03	0.30625	0	0	2.72E-04	
8	7.50E-03	0.3075	0	0	2.70E-04	
9	8.75E-03	0.30875	0	0	2.68E-04	
10	1.00E-02	0.31	0	0	2.66E-04	
11	1.13E-02	0.31125	0	0	2.64E-04	
12	1.25E-02	0.3125	0	0	2.63E-04	
13	1.38E-02	0.31375	0	0	2.61E-04	
14	1.50E-02	0.315	0	0	2.60E-04	
15	1.63E-02	0.31625	0	0	2.58E-04	
16	1.75E-02	0.3175	0	0	2.57E-04	
17	1.88E-02	0.31875	0	0	2.55E-04	

Figure 3.22: The Data Extracted from the FEA.

3.5 Summary

At this point, all three sets of results were obtained from three separate sources. The results will be cross-checked to verify the validity of the analytical solution. If the solution fails this test, it could be inferred that there is a mistake either in the derivation of the solution, in the code written in MATLAB, or in the boundary conditions in the FEA model. Any discrepancies in the results will have to be studied to find the source of the error.

CHAPTER 4

RESULTS AND DISCUSSION

4.1 Introduction

After completing all the preceding steps in the previous chapter, the results collected from all three sources can be collected and compared. The proposed analytical solution would first be compared to the reference paper, followed by a comparison with the FEA results. Then, further studies can be done to investigate the rate of convergence of the proposed solution, as well as a parametric study to observe the effects of varying parameters on the pressure vessel.

4.2 Results Verification

4.2.1 Results Verification with Literature

The results from the proposed analytical solution was recorded in an Excel spreadsheet, along with the extracted results from Bayat et al. (2011). Figure 4.1 below shows the graphs plotted from the results. For the graphs of radial and tangential stresses, the y-axis used is normalized. Instead of normalizing by dividing each data point by the largest value, they were divided by the internal load, i.e. each data point was divided by 80 MPa. This makes it easier to compare the applied load to the stresses induced within the pressure vessel.

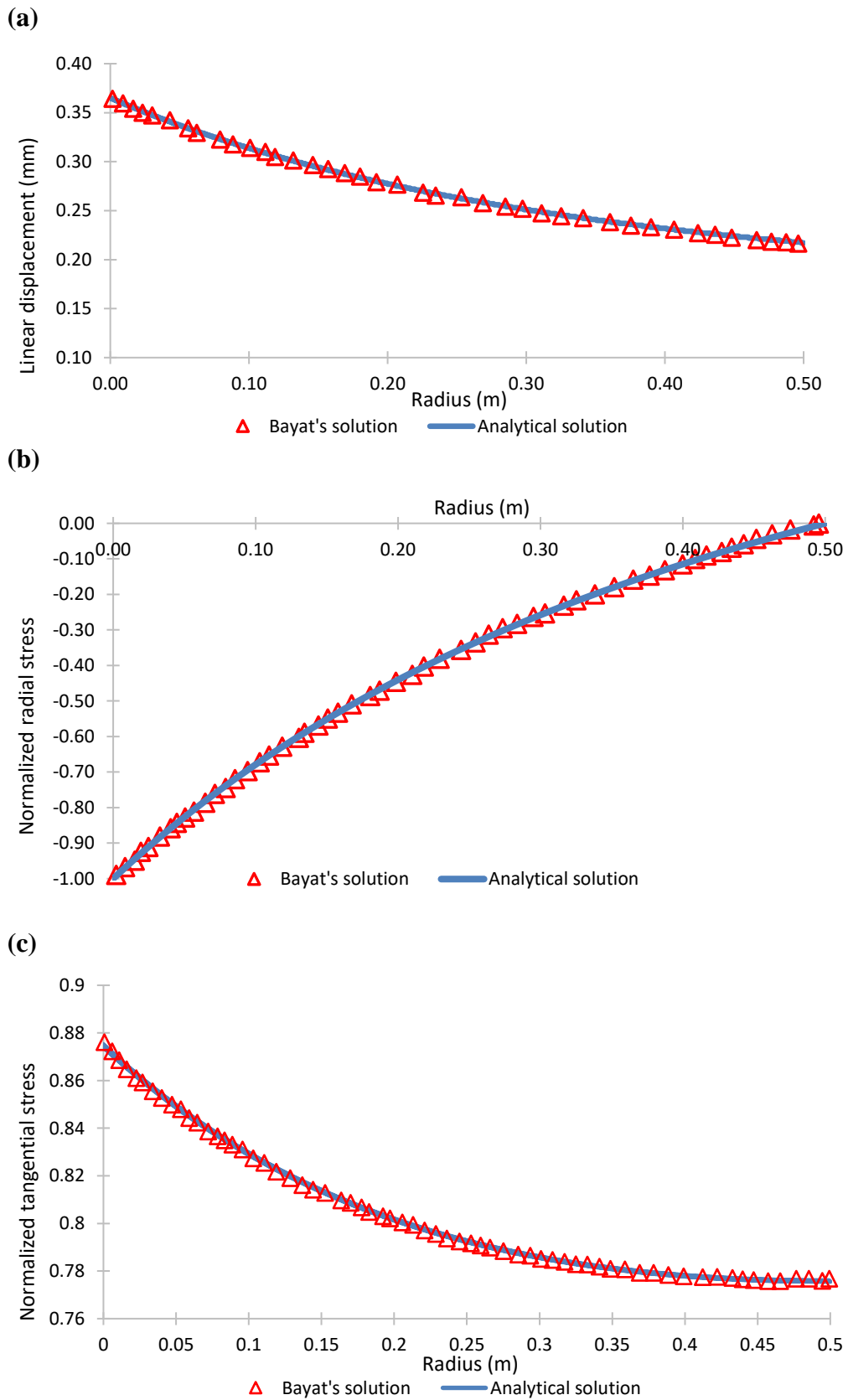


Figure 4.1: Graphs Plotted for the Analytical Solution and the Results Produced by Bayat for (a) Linear Displacement, (b) Radial Stress, and (c) Tangential Stress.

From Figure 4.1, it is observed that the results from the proposed analytical solution are nearly identical to the results from the reference paper. The results verification with Bayat's solution is a success, whereby the average percentage error in this comparison was only 1.5%.

4.2.2 Results Verification with FEA Outcome

The FEA model was constructed according to the procedures described in Chapter 3.6. The material properties for each layer were manually defined in the Engineering Data section according to Equation (3.27), which defines the elastic modulus as a function of radius. The Poisson's ratio was constant throughout all layers, at $\nu = 0.3$.

As mentioned in the previous chapter, a 20 layered spherical model was used instead of a proper FGM structure, because ANSYS does not currently support the use of FGM in modelling.

The comparison between this set of results and the proposed solution is very close, as seen in Figure 4.2 below. For these graphs, the x-axis for the graphs was replaced with the thickness ratio of the vessel wall, where the innermost surface of the vessel is zero, while the outermost surface is one.

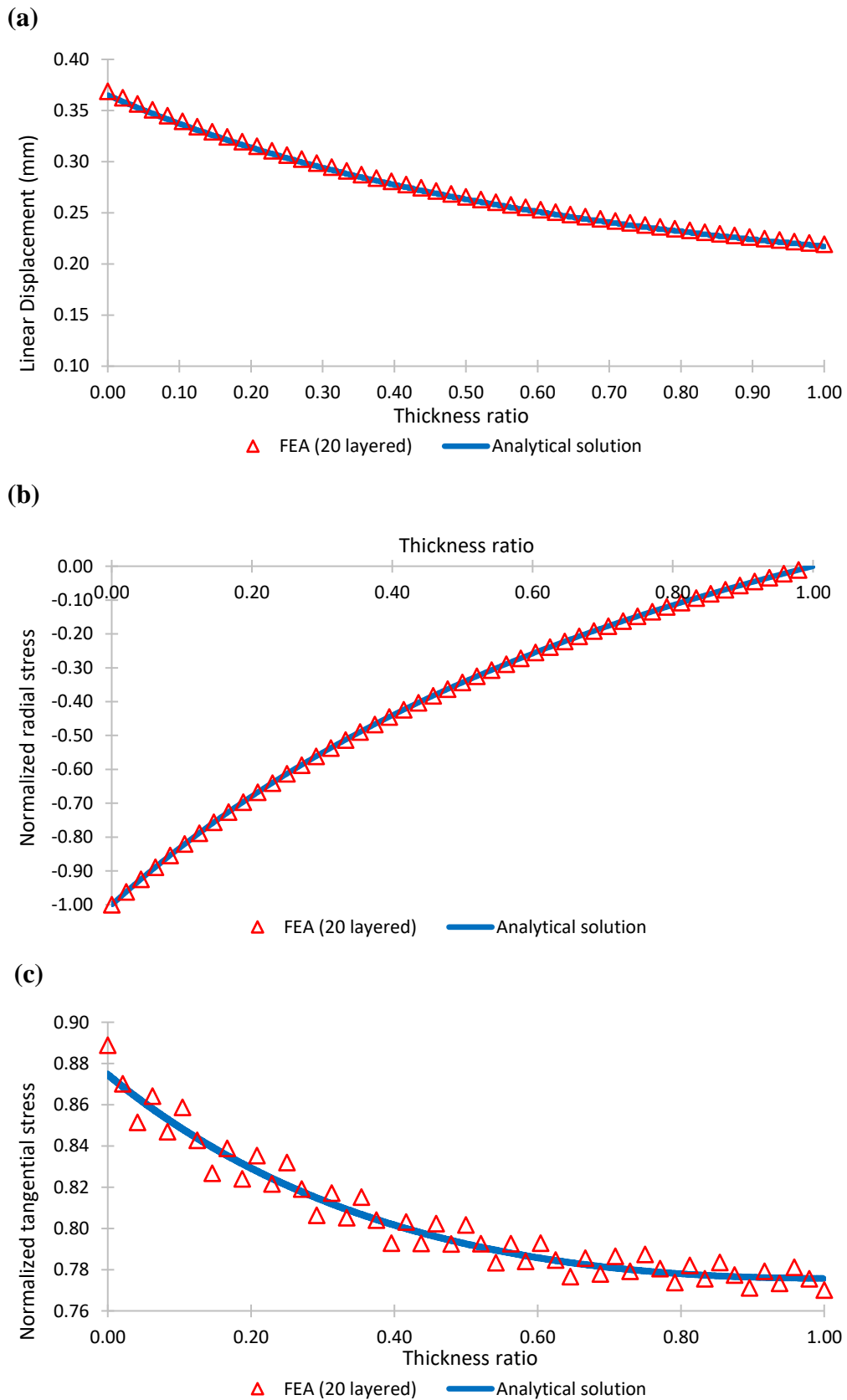


Figure 4.2: Graphs Plotted for the Analytical Solution and the Results Produced by the FEA for (a) Linear Displacement, (b) Radial Stress, and (c) Tangential Stress.

From Figure 4.2, the verification with FEA simulation is also a success. This comparison has yielded a percentage error of a mere 0.5%.

4.3 Convergence Study

Now that the accuracy of the proposed solution has been verified against both a reference paper as well as an FEA, further work can be done on this algorithm to improve on its precision. A convergence study was carried out with the purpose of determining the minimum number of layers required to produce a satisfactory curve.

Because the proposed solution relies on modelling FGM structures as multilayered structures, there would be a noticeable “leap” in the curve between one layer and the next. This is due to the abrupt shift in mechanical properties when one material transitions into the next.

Increasing the number of layers in the models can reduce this effect to a minimum. When the number of layers is sufficiently high, each individual layer becomes much thinner. In this case, the shift in mechanical properties, will be much smaller. In other words, the models should have enough layers so that the resulting curves would look smooth enough to be considered as a continuous curve.

Figure 4.3 below shows the comparison between Bayat’s results and the proposed analytical solution modelled as 50 layers.

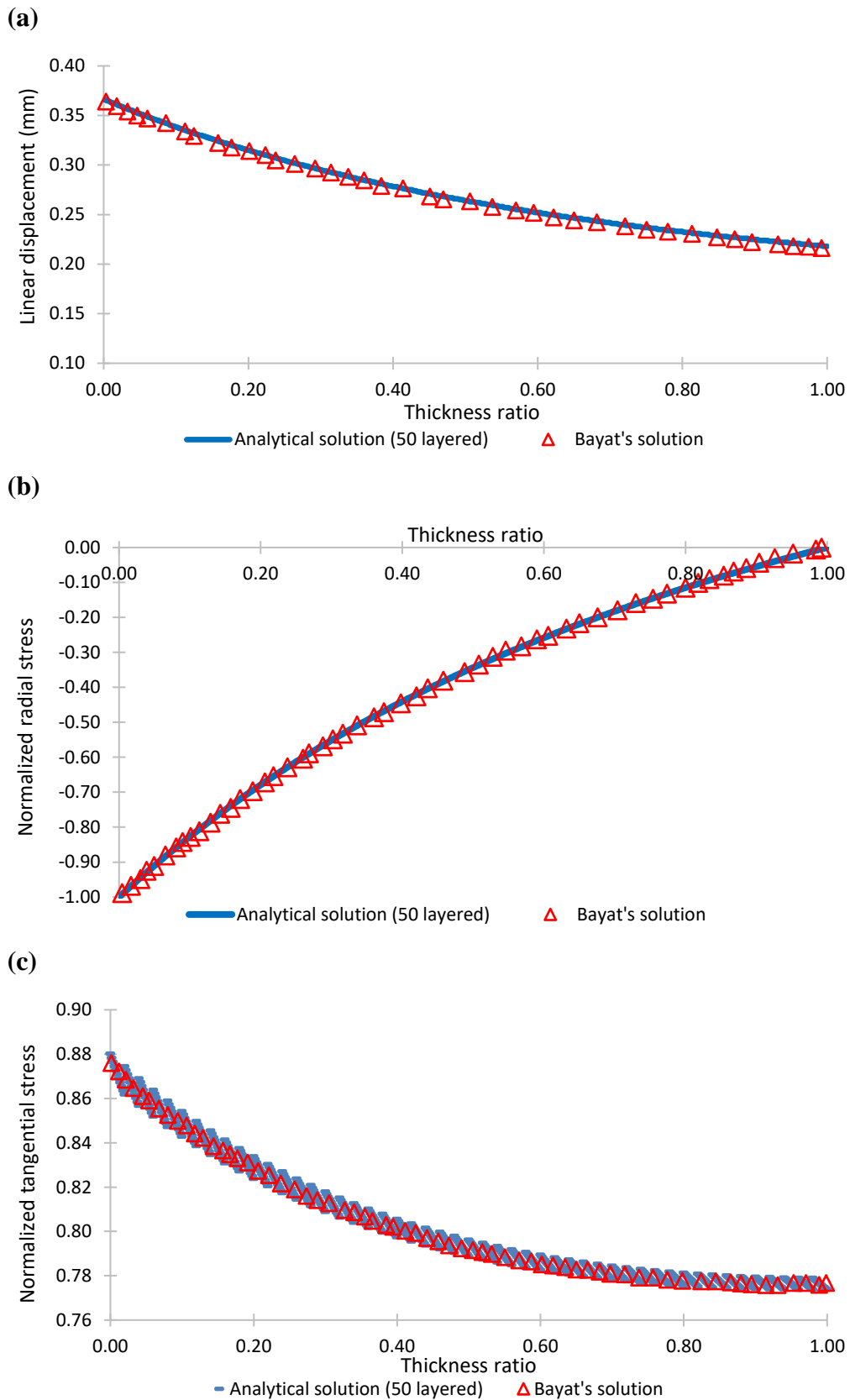


Figure 4.3: Graphs Plotted for the Analytical Solution (50 layered) and the Results Produced by Bayat et al. (2011) for (a) Linear Displacement, (b) Radial Stress, and (c) Tangential Stress.

The graphs for linear displacement in Figure 4.3(a) and radial stress in Figure 4.3(b) are both continuous, resulting in a very accurate outcome. However, the tangential stress curve in Figure 4.3(c) is discontinuous. The analytical solution produces results that highly resemble Bayat's solution, but with a very noticeable gap at the interfaces between layers. The proposed solution was run again at a higher layer count to observe the differences between a 50 layered model and a 500 layered model. The results were plotted in Figure 4.4.

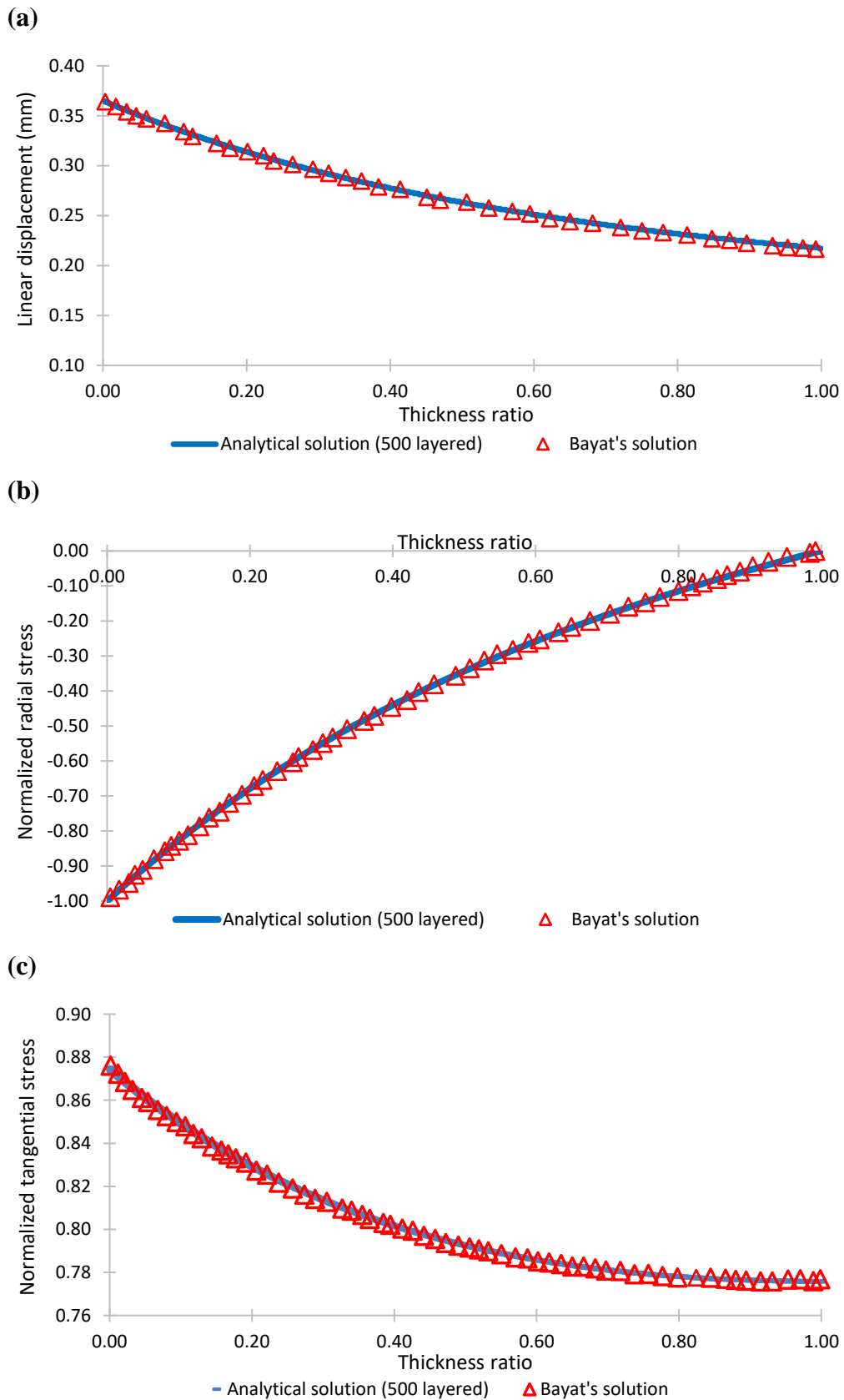


Figure 4.4: Graphs Plotted for the Analytical Solution (500 layered) and the Results Produced by the FEA for (a) Linear Displacement, (b) Radial Stress, and (c) Tangential Stress.

As seen in Figure 4.4 above, when the 50 layered model was replaced with a 500 layered model, the continuous curves for linear displacement in Figure 4.4(a) and radial stress in Figure 4.4(b) remained almost exactly the same as in Figure 4.3. There is no meaningful improvement observed. On the other hand, the tangential stress curve in Figure 4.4(c) was greatly improved, where the gaps between layers were reduced drastically. The discontinuities in the graph were no longer noticeable unless zoomed very far in.

Observing Figures 4.3 and 4.4, it is concluded that for continuous curves such as the linear displacement and radial stress, a 50 layered model is sufficient. The tangential stress curve, however, is not ideal. A 500 layered model is recommended to obtain much more respectable results.

One issue with increasing the number of layers is the waste in computing power, especially since the starting point of this project was to develop a mathematical model that saves computing power in the first place. That said, even with the solution configured to a 5000 layered model, the process of solving the model was still completed in less than 10 seconds, even on old hardware. Thus, it can be concluded that computing power is not a limitation in this case.

Another minor problem with a very high layer count is the large number of data points. Too many data points might result in a bloated graph that can be difficult to understand, especially if there are multiple curves in the same graph. This problem can be easily mitigated by selectively excluding some of the data points.

4.4 Parametric Study

The purpose of carrying out this parametric study was to investigate how the mechanical properties and the loading conditions would affect the performance of the pressure vessel. Referring to the convergence study, a model of 500 layers was to be used for this portion of the project. All figures in the parametric study was produced using a 500 layered model.

4.4.1 Varying the Elastic Modulus

The first parameter to be studied was the elastic modulus. The elastic modulus at every point in the model was increased in increments of 25 GPa, up to a maximum of 125 GPa. The solution was rerun after every change and the results recorded. Figure 4.5 shows the changes in the linear displacement graph.

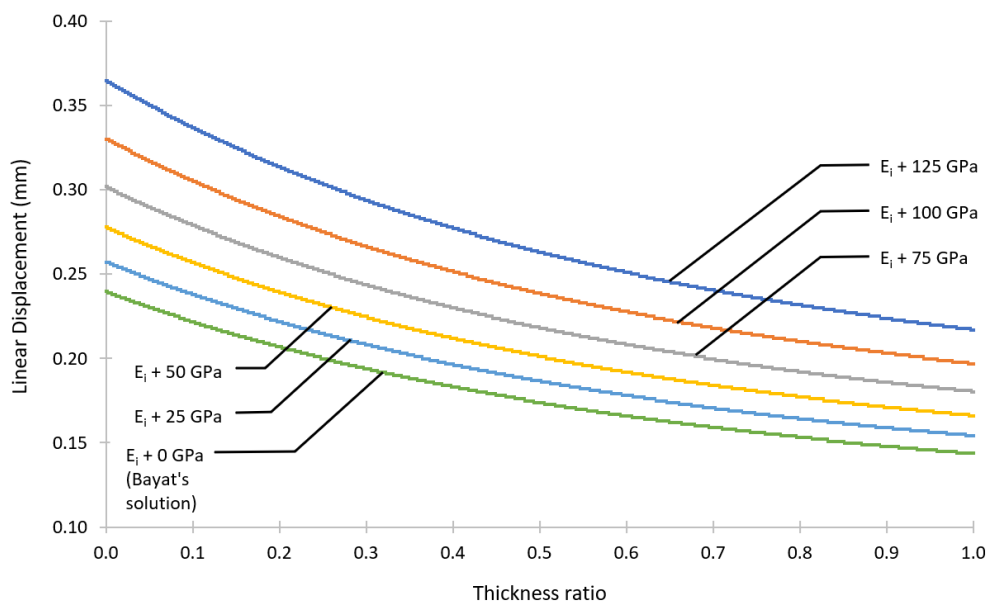


Figure 4.5: The Effects of an Increasing Elastic Modulus on the Graph of Linear Displacement against Thickness Ratio.

The improvements to linear displacement from increasing the elastic modulus is very straightforward: the displacement becomes smaller, and the entire graph shifts downward. This effect also has diminishing returns, where the improvements become less and less significant even though the elastic modulus continues to increase by a fixed amount. In other words, the constant increment of 25 GPa does not contribute to an improvement of a fixed amount.

Figure 4.6 below shows the changes in the radial stress.

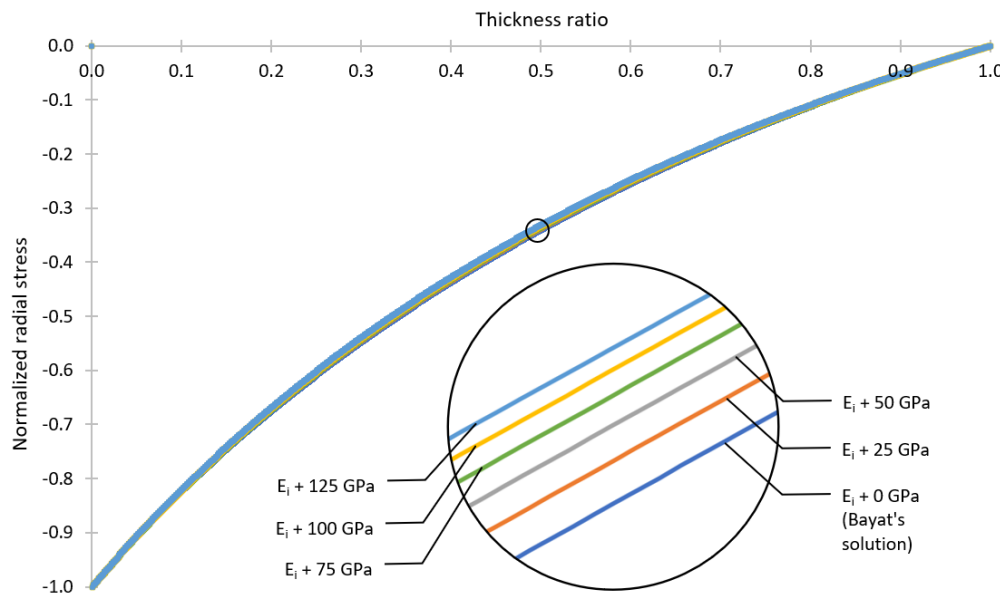


Figure 4.6: The Effects of an Increasing Elastic Modulus on the Graph of Normalized Radial Stress against Thickness Ratio.

The radial stress at both the innermost and outermost layers remain constant regardless of the changes in the elastic modulus. This is because the two boundary layers are directly exposed to the internal and external pressures. However, the curve does have a steeper gradient at the inner layers and a flatter gradient at the outer layers. Overall, the effects of varying the elastic modulus on the radial stress of the model is insignificant.

Figure 4.7 is the graph plotted for the tangential stress.

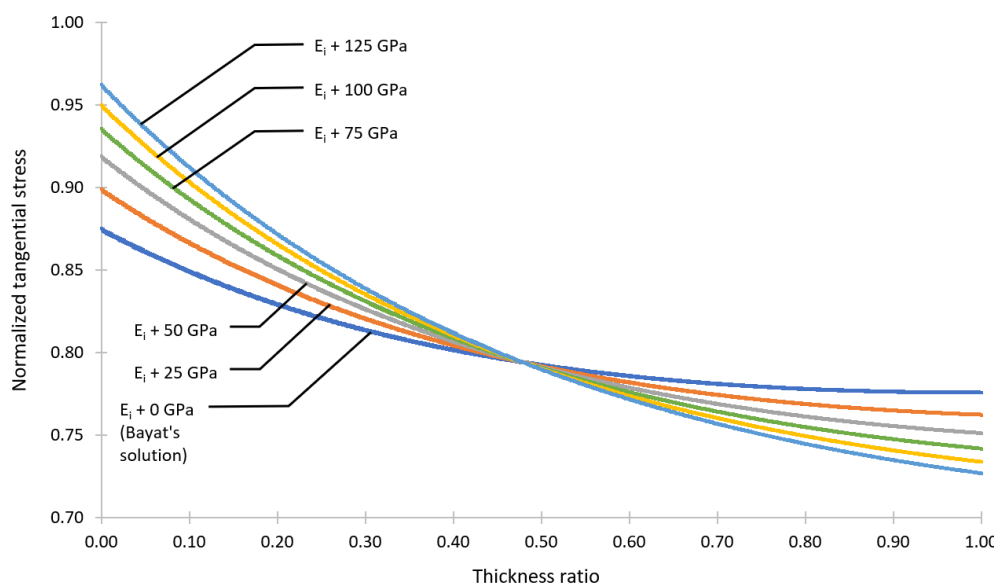


Figure 4.7: The Effects of an Increasing Elastic Modulus on the Graph of Normalized Tangential Stress against Thickness Ratio.

From the output, it was observed that as the elastic modulus increases, the maximum value in the tangential stress curve increases, while at the same time the minimum value decreases. When the material is stiffer, less of the stress will be transmitted further down to the next layer, which results in a larger gap between the maximum and minimum tangential stress. Similar to the radial displacement graph, this effect also has diminishing returns.

Overall, this trend indicates that employing the use of stiffer materials would be conducive in minimizing the deformation of pressure vessels while under load, at the expense of an increased maximum tangential stress.

4.4.2 Varying the Loading Pressure

Other than the mechanical properties of the vessel itself, another important parameter is the loading conditions of the structure. The material choices made while designing a pressure vessel will be directly correlated to its expected loading conditions. As expected, the vessels will be under larger stresses when there is a larger load. Thus, the internal loading of the model was increased with increments of 20 MPa, up to a maximum of 160 MPa.

However, when a different loading was applied to the model, the graphs for both radial and tangential stresses remain completely unchanged. This is because the y-axis in these graphs were normalized. The stresses were divided by the load applied. This also means the stresses scale very well to the amount of load applied to the model. The linear displacement, however, was not normalized. The effects of a higher loading can be clearly seen in Figure 4.8

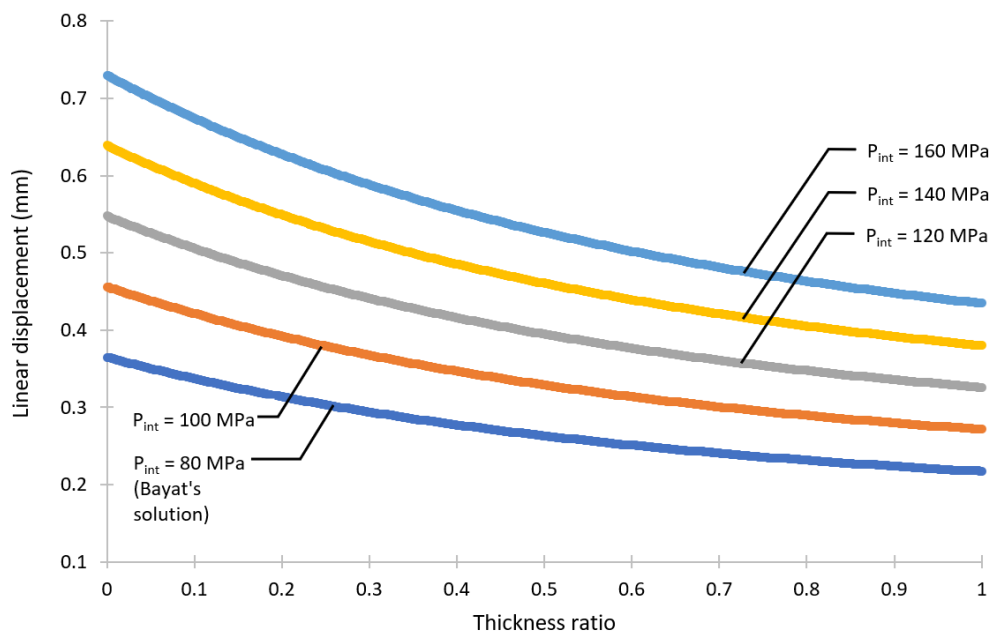


Figure 4.8: The Effects of an Increasing Load on the Graph of Linear Displacement against Thickness Ratio.

Unsurprisingly, the displacement increases when the loading increases. However, unlike in the previous subsection where the elastic modulus was varied, the continuous increase in displacement does not appear to slow down as the load was increased by a fixed amount.

Because of this trend, it is safe to assume that the linear displacement curve scales linearly with respect to the pressure exerted on its interior surface.

4.4.3 Varying the Wall Thickness

One of the most straightforward ways of strengthening a pressure vessel is to simply increase its thickness. For this part, the thickness was varied by either increasing or decreasing the ratio of outer radius to inner radius. The original ratio was 1.5. A thicker vessel would have a larger ratio. Ratios of 1.25, 1.75, 2.0, and 2.25 were tested and the results were shown in Figure 4.9.

Despite having different radii, these curves are still comparable because the x-axis is defined as the normalized thickness ratio, where every point was divided by its maximum value.

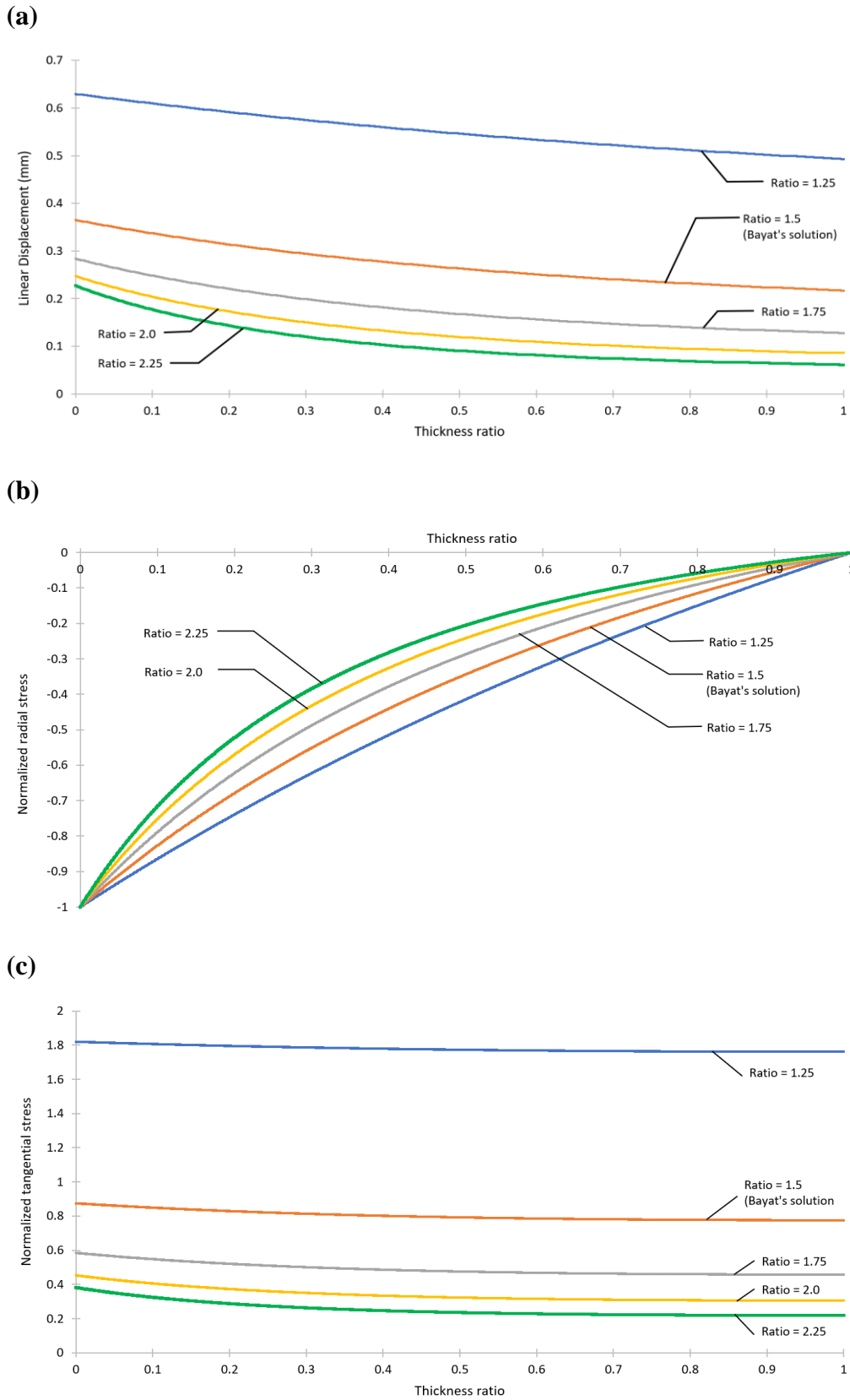


Figure 4.9: The Effects of Varying Wall Thickness for the Graphs of (a) Linear Displacement, (b) Normalized Radial Stress, and (c) Normalized Tangential Stress.

The stress distribution of the pressure vessel is significantly improved by increasing thickness of the vessel wall. Both stresses as well as the displacement were reduced by a wide margin. Again, the improvements diminished rapidly. Further thickening the vessel no longer yielded similarly obvious improvements.

On the other hand, when the thickness was reduced, both the linear displacement and the tangential stress dramatically increased. Their magnitudes were almost doubled with just a 16.7% reduction in thickness.

From the trend, it is observed that out of all the parameters considered, the thickness of the pressure vessel gives the greatest improvements on its performance. However, an increased thickness will contribute to a higher manufacturing cost, lower space efficiency, and increased weight. These are all significant drawbacks that will directly contribute to higher overall costs. With that in mind, increasing the thickness of the wall is likely not a very practical way to strengthen the pressure vessel.

4.5 Observations from the Study

The prediction made at the beginning of this project has proved to be correct: running the proposed solution via MATLAB is a much quicker way to solve for the stresses than running FEA. This is especially true if one or more parameters have to be constantly manipulated, such as during the design phase of a particular pressure vessel configuration.

Whenever the situation requires the user to trial and error, running the analytical solution instead of the FEA allows the user to make quick minor corrections to the setup before every run. On the other hand, FEA would require a longer time to rerun the simulation, and in some cases might even require remeshing the structure if the dimensions were altered, which is not necessary for the analytical solution. Other than that, the analytical solution is much less demanding on the hardware requirements, which also results in a shorter runtime.

Ultimately, both applications have their respective strengths and weaknesses. A Finite Element Analysis is more useful, more flexible, and more suitable for one-off situations where only one model will be simulated. The

analytical solution is more suitable for design work, or even for studies such as the parametric study conducted in this project.

CHAPTER 5

CONCLUSIONS AND RECOMMENDATIONS

5.1 Conclusions

In this project, an analytical solution has been successfully developed for the mechanical stress distribution of a multilayered spherical pressure vessel. The project objectives have been achieved where:

- To derive the analytical solution for the mechanical stresses of a spherical pressure vessel, starting from the stress-strain relation equations for spherical structures.
- To program the solution into MATLAB and run the solution with a predefined set of material properties and loading conditions.
- To verify the accuracy of the proposed solution by comparing it to the results obtained from a 2D FEA simulation, as well as a set of reference results from a suitable and reliable external source.

Overall, the results obtained from running the proposed solution has proved to be highly successful. They are in agreement with the output from a 2D Finite Element Analysis, with an average error of 0.5%. With reference to Bayat et al. (2011), the pressure vessel proposed by the paper was modelled using the proposed solution. Again, the results from both sources are in agreement, with an average error of 1.5%.

From the convergence study, it was concluded that FGM pressure vessels should be modelled with 500 layers to ensure the smoothness of the output curves. Parameters that are considered in the parametric study are the elastic modulus, the loading pressure, and the thickness of the pressure vessel. These parameters each have their unique effects on the performance of the pressure vessels. In general, significant improvements were observed from increasing the elastic modulus, decreasing the loading pressure, or increasing the wall thickness. However, most of these improvements diminish as the changes were scaled further. A fixed increase of 25 GPa in the material's elastic

modulus may result in a reduction of 10% for the linear displacement for the first run, but further increasing it will only provide improvements less than 10%.

5.2 Recommendations for Future Work

The main omission in the proposed solution is the aforementioned thermal effects. As explained in the limitations section, thermal stress tends to overwhelm mechanical stresses when the structure reaches high temperatures. Therefore, the thermal effects ought not to be overlooked if the intended purpose of the pressure vessel is to transport fluids at elevated temperatures. This is often the case in commercial uses, since a high pressure is usually correlated with a high temperature.

In its present state, this solution will provide the same results for two identical pressure vessels but at different temperatures. Thus, there is room to extend the work done on this project to overcome this limitation.

A more comprehensive solution can be developed by including the thermal term into the stress-strain relation equations. This term can be modelled as a function of the elastic modulus, the Poisson's ratio, and the thermal conductivity of the material in question. The derivation will be more complicated than before, but the basic concept of the project remains the same.

REFERENCES

Bayat, Y., Ghannad, M. & Torabi, H., 2012. Analytical and numerical analysis for the FGM thick sphere under combined pressure and temperature loading. *Archive of Applied Mechanics*, 82(2), pp. 229-242.

Brischetto, S., 2017. Exact three-dimensional static analysis of single- and multi-layered plates and shells. *Composites Part B: Engineering*, Volume 119, pp. 230-252.

Brownlee, J., 2018. *Analytical vs Numerical Solutions in Machine Learning*. [Online]
Available at: <https://machinelearningmastery.com/analytical-vs-numerical-solutions-in-machine-learning/>
[Accessed 11 May 2020].

Darijani, H., Kargarnovin, M. H. & Naghdabadi, R., 2009. Design of spherical vessels under steady-state thermal loading using thermo-elasto-plastic concept. *International Journal of Pressure Vessels and Piping*, 86(2-3), pp. 143-152.

Dubal, S. & Kadam, H., 2017. Pressure Vessel Accidents: Safety Approach. *International Research Journal of Engineering and Technology (IRJET)*, 7(1), pp. 125-128.

Fukui, Y. & Yamanaka, N., 1992. Elastic Analysis for Thick-Walled Tubes of Functionally Graded Material Subjected to Internal Pressure. *JSME International Journal: Solid mechanics*, 35(4), pp. 379-385.

Kalanta, S., Atkočiūnas, J. & Ulitinas, T., 2013. Equilibrium Finite Elements of Spherical Shells in Analysis Problems. *Procedia Engineering*, Volume 57, pp. 515-523.

Kashtalyan, M., 2004. Three-dimensional elasticity solution for bending of functionally graded rectangular plates. *European Journal of Mechanics - A/Solids*, 23(5), pp. 853-864.

Khorsand, M. & Tang, Y., 2019. Thermal analysis and electro-elastic response of multilayered spherical vessels. *International Journal of Pressure Vessels and Piping*, Volume 171, pp. 194-206.

Li, P., Petrinic, N. & Siviour, C. R., 2012. Finite element modelling of the mechanism of deformation and failure in metallic thin-walled hollow spheres under dynamic compression. *Mechanics of Materials*, Volume 54, pp. 43-54.

Livingston, E. & Scavuzzo, R. J., 2000. Pressure Vessels. In: *Pressure Vessels: The Engineering Handbook*. Boca Raton: CRC Press LLC.

Moita, J. S., Mota Soares, C. M., Mota Soares, C. A. & Ferreira, A. J. M., 2019. Elastoplastic and nonlinear analysis of functionally graded axisymmetric shell structures under thermal environment, using a conical frustum finite element model. *Composite Structures*, Volume 226.

More, S. T. & Bindu, R. S., 2015. Effects of Mesh Size on Finite Element Analysis of Plate Structure. *International Journal of Engineering Science and Innovative Technology (IJESIT)*, 4(3), pp. 181-185.

Mukherjee, R., 2019. Reimagining pressure vessels in the 21st century. *Reinforced Plastics*, 63(3), pp. 143-145.

Shi, Z., Zhang, T. & Xiang, H., 2006. Exact solutions of heterogeneous elastic hollow cylinders. *Composite Structures*, 79(1), pp. 140-147.

Somadder, S. & Islam, M. S., 2015. Stress Analysis of a Cylinder Subjected to Thermo-mechanical Loads by using FEM. *IOP Conference Series: Materials Science and Engineering*, 438(1), pp. 1-8.

Sundar, U. M., 2012. *Mathematical Modeling using MATLAB*. [Online] Available at:

<https://www.mathworks.com/content/dam/mathworks/mathworks-dot-com/solutions/automotive/files/in-expo-2012/mathematical-modelling-using-matlab.pdf>

Thomson, J. R., 2015. Chapter 7 - Learning from Ignorance: A Brief History of Pressure Vessel Integrity and Failures. *High Integrity Systems and Safety Management in Hazardous Industries*, pp. 99-125.

Tutuncu, N. & Ozturk, M., 2001. Exact solutions for stresses in functionally graded pressure vessels. *Composites Part B: Engineering*, 32(8), pp. 683-686.

Tutuncu, N. & Temel, B., 2009. A novel approach to stress analysis of pressurized FGM cylinders, disks and spheres. *Composite Structures*, 91(3), pp. 385-390.

Zhang, Q. et al., 2012. Analytical solution of the thermo-mechanical stresses in a multilayered composite pressure vessel considering the influence of the closed ends. *International Journal of Pressure Vessels and Piping*, Volume 98, pp. 102-110.

Zheng, C., Li, X. & Mi, C., 2019. Reducing stress concentrations in unidirectionally tensioned thick-walled spheres through embedding a functionally graded reinforcement. *International Journal of Mechanical Sciences*, Volume 152, pp. 257-267.

Zienkiewicz, O. C., Taylor, R. L. & Zhu, J. Z., 2013. *The Finite Element Method: Its Basis and Fundamentals*. 7th ed. Oxford: Butterworth-Heinemann.

APPENDICES

APPENDIX A: Results Verification Comparisons

Table A-1: Comparison between the Proposed Analytical Solution and the Reference Solution for the Linear Displacement.

Layer	Inner	Outer	Linear displacement (mm)		
	radius (m)	radius (m)	Bayat's solution	Analytical solution	Error (%)
1	0.000	0.025	0.34	0.35	2.94
2	0.025	0.050	0.34	0.34	0.00
3	0.050	0.075	0.32	0.33	3.13
4	0.075	0.100	0.31	0.31	0.00
5	0.100	0.125	0.30	0.30	0.00
6	0.125	0.150	0.29	0.29	0.00
7	0.150	0.175	0.28	0.28	0.00
8	0.175	0.200	0.27	0.28	3.70
9	0.200	0.225	0.27	0.27	0.00
10	0.225	0.250	0.26	0.26	0.00
11	0.250	0.275	0.25	0.25	0.00
12	0.275	0.300	0.25	0.25	0.00
13	0.300	0.325	0.24	0.24	0.00
14	0.325	0.350	0.24	0.24	0.00
15	0.350	0.375	0.23	0.23	0.00
16	0.375	0.400	0.23	0.23	0.00
17	0.400	0.425	0.22	0.22	0.00
18	0.425	0.450	0.22	0.22	0.00
19	0.450	0.475	0.21	0.22	4.76
20	0.475	0.500	0.21	0.21	0.00
			Average		0.73

Table A-2: Comparison between the Proposed Analytical Solution and the Reference Solution for the Normalized Radial Stress.

Layer	Inner	Outer	Normalized radial stress		
	radius (m)	radius (m)	Bayat's solution	Analytical solution	Error (%)
1	0.000	0.025	-0.91	-0.91	0.00
2	0.025	0.050	-0.84	-0.84	0.00
3	0.050	0.075	-0.76	-0.76	0.00
4	0.075	0.100	-0.69	-0.69	0.00
5	0.100	0.125	-0.62	-0.62	0.00
6	0.125	0.150	-0.56	-0.56	0.00
7	0.150	0.175	-0.50	-0.51	2.00
8	0.175	0.200	-0.44	-0.44	0.00
9	0.200	0.225	-0.40	-0.40	0.00
10	0.225	0.250	-0.35	-0.35	0.00
11	0.250	0.275	-0.29	-0.30	3.45
12	0.275	0.300	-0.26	-0.26	0.00
13	0.300	0.325	-0.23	-0.23	0.00
14	0.325	0.350	-0.20	-0.19	5.00
15	0.350	0.375	-0.15	-0.16	6.67
16	0.375	0.400	-0.11	-0.11	0.00
17	0.400	0.425	-0.09	-0.09	0.00
18	0.425	0.450	-0.05	-0.06	20.00
19	0.450	0.475	-0.03	-0.04	33.33
20	0.475	0.500	0.00	0.00	0.00
			Average		3.52

Table A-3: Comparison between the Proposed Analytical Solution and the Reference Solution for the Normalized Tangential Stress.

Layer	Inner	Outer	Normalized tangential stress		
	radius (m)	radius (m)	Bayat's solution	Analytical solution	Error (%)
1	0.000	0.025	0.86	0.86	0.00
2	0.025	0.050	0.84	0.85	1.19
3	0.050	0.075	0.83	0.84	1.20
4	0.075	0.100	0.83	0.83	0.00
5	0.100	0.125	0.82	0.82	0.00
6	0.125	0.150	0.81	0.81	0.00
7	0.150	0.175	0.80	0.80	0.00
8	0.175	0.200	0.80	0.80	0.00
9	0.200	0.225	0.79	0.79	0.00
10	0.225	0.250	0.79	0.79	0.00
11	0.250	0.275	0.78	0.79	1.28
12	0.275	0.300	0.78	0.78	0.00
13	0.300	0.325	0.78	0.78	0.00
14	0.325	0.350	0.78	0.78	0.00
15	0.350	0.375	0.77	0.77	0.00
16	0.375	0.400	0.77	0.77	0.00
17	0.400	0.425	0.77	0.77	0.00
18	0.425	0.450	0.77	0.77	0.00
19	0.450	0.475	0.77	0.77	0.00
20	0.475	0.500	0.77	0.77	0.00
			Average		0.18

Table A-4: Comparison between the Proposed Analytical Solution and the Finite Element Analysis for the Linear Displacement.

Layer	Inner radius (m)	Outer radius (m)	Linear displacement (mm)		Error (%)
			FEA	Analytical solution	
1	0.000	0.025	0.35	0.35	0.00
2	0.025	0.050	0.34	0.34	0.00
3	0.050	0.075	0.32	0.32	0.00
4	0.075	0.100	0.31	0.31	0.00
5	0.100	0.125	0.30	0.30	0.00
6	0.125	0.150	0.29	0.29	0.00
7	0.150	0.175	0.29	0.28	3.45
8	0.175	0.200	0.28	0.27	3.57
9	0.200	0.225	0.27	0.27	0.00
10	0.225	0.250	0.26	0.26	0.00
11	0.250	0.275	0.26	0.25	3.85
12	0.275	0.300	0.25	0.25	0.00
13	0.300	0.325	0.24	0.24	0.00
14	0.325	0.350	0.24	0.24	0.00
15	0.350	0.375	0.23	0.23	0.00
16	0.375	0.400	0.23	0.23	0.00
17	0.400	0.425	0.23	0.22	4.35
18	0.425	0.450	0.22	0.22	0.00
19	0.450	0.475	0.22	0.22	0.00
20	0.475	0.500	0.21	0.21	0.00
Average					0.76

Table A-5: Comparison between the Proposed Analytical Solution and the Finite Element Analysis for the Normalized Radial Stress.

Layer	Inner radius (m)	Outer radius (m)	Normalized radial stress		
			FEA	Analytical solution	Error (%)
1	0.000	0.025	-0.92	-0.92	0.00
2	0.025	0.050	-0.85	-0.85	0.00
3	0.050	0.075	-0.75	-0.75	0.00
4	0.075	0.100	-0.69	-0.69	0.00
5	0.100	0.125	-0.61	-0.61	0.00
6	0.125	0.150	-0.56	-0.56	0.00
7	0.150	0.175	-0.51	-0.51	0.00
8	0.175	0.200	-0.44	-0.44	0.00
9	0.200	0.225	-0.40	-0.40	0.00
10	0.225	0.250	-0.34	-0.34	0.00
11	0.250	0.275	-0.30	-0.30	0.00
12	0.275	0.300	-0.27	-0.27	0.00
13	0.300	0.325	-0.22	-0.22	0.00
14	0.325	0.350	-0.19	-0.19	0.00
15	0.350	0.375	-0.14	-0.14	0.00
16	0.375	0.400	-0.12	-0.12	0.00
17	0.400	0.425	-0.09	-0.09	0.00
18	0.425	0.450	-0.05	-0.05	0.00
19	0.450	0.475	-0.03	-0.03	0.00
20	0.475	0.500	0.00	0.00	0.00
Average					0.00

Table A-6: Comparison between the Proposed Analytical Solution and the Finite Element Analysis for the Normalized Tangential Stress.

Layer	Inner radius (m)	Outer radius (m)	Normalized tangential stress		
			FEA	Analytical solution	Error (%)
1	0.000	0.025	0.85	0.86	1.18
2	0.025	0.050	0.84	0.85	1.19
3	0.050	0.075	0.82	0.83	1.22
4	0.075	0.100	0.82	0.83	1.22
5	0.100	0.125	0.83	0.82	1.20
6	0.125	0.150	0.80	0.81	1.25
7	0.150	0.175	0.80	0.80	0.00
8	0.175	0.200	0.79	0.80	1.27
9	0.200	0.225	0.79	0.79	0.00
10	0.225	0.250	0.80	0.79	1.25
11	0.250	0.275	0.78	0.78	0.00
12	0.275	0.300	0.78	0.78	0.00
13	0.300	0.325	0.77	0.78	1.30
14	0.325	0.350	0.77	0.78	1.30
15	0.350	0.375	0.78	0.77	1.28
16	0.375	0.400	0.77	0.77	0.00
17	0.400	0.425	0.77	0.77	0.00
18	0.425	0.450	0.77	0.77	0.00
19	0.450	0.475	0.77	0.77	0.00
20	0.475	0.500	0.77	0.77	0.00
Average					0.68

Calculations for the Average Error

For the comparison between the proposed analytical solution and the reference paper, the average error is

$$\begin{aligned} \text{Average Error} &= \frac{(0.73 + 3.52 + 0.18)}{3} \\ \text{Average Error} &= 1.48\% \approx 1.5\% \end{aligned}$$

For the comparison between the proposed analytical solution and the FEA results, the average error is

$$\begin{aligned} \text{Average Error} &= \frac{(0.76 + 0.00 + 0.68)}{3} \\ \text{Average Error} &= 0.48\% \approx 0.5\% \end{aligned}$$

APPENDIX B: Originality Report

FYP2

ORIGINALITY REPORT

2%

SIMILARITY INDEX

1%

INTERNET SOURCES

1%

PUBLICATIONS

1%

STUDENT PAPERS

PRIMARY SOURCES

1	Submitted to Universiti Tunku Abdul Rahman Student Paper	<1%
2	Z.S. Shao, G.W. Ma. "Thermo-mechanical stresses in functionally graded circular hollow cylinder with linearly increasing boundary temperature", Composite Structures, 2008 Publication	<1%
3	Zhenyue Zhang. "Stability and Fast Algorithms of Incomplete LU Factorization with Zero-Fill for Nine-Diagonal Matrices", SIAM Journal on Matrix Analysis and Applications, 2007 Publication	<1%
4	eprints.utar.edu.my Internet Source	<1%
5	Naki Tutuncu, Beytullah Temel. "An Efficient Unified Method for Thermoelastic Analysis of Functionally Graded Rotating Disks of Variable Thickness", Mechanics of Advanced Materials and Structures, 2013 Publication	<1%

APPENDIX C: Comment on Originality Report

Universiti Tunku Abdul Rahman			
Form Title : Supervisor's Comments on Originality Report Generated by Turnitin for Submission of Final Year Project Report (for Undergraduate Programmes)			
Form Number: FM-IAD-005	Rev No.: 0	Effective Date: 01/10/2013	Page No.: 67 of 1



FACULTY OF ENGINEERING AND SCIENCE

Full Name(s) of Candidate(s)	Ng Yee Ping
ID Number(s)	1506297
Programme / Course	Bachelor in Engineering (Honours.) Mechanical Engineering
Title of Final Year Project	Analytical solution for the mechanical stresses of multilayered hollow spherical pressure vessel.

Similarity	Supervisor's Comments (Compulsory if parameters of originality exceeds the limits approved by UTAR)
Overall similarity index: 2 % Similarity by source Internet Sources: 1 % Publications: 1 % Student Papers: 1 %	O.K
Number of individual sources listed of more than 3% similarity: 0	O.K
Parameters of originality required and limits approved by UTAR are as follows: (i) Overall similarity index is 20% and below, and (ii) Matching of individual sources listed must be less than 3% each, and (iii) Matching texts in continuous block must not exceed 8 words <i>Note: Parameters (i) – (ii) shall exclude quotes, bibliography and text matches which are less than 8 words.</i>	

Note Supervisor/Candidate(s) is/are required to provide softcopy of full set of the originality report to Faculty/Institute

Based on the above results, I hereby declare that I am satisfied with the originality of the Final Year Project Report submitted by my student(s) as named above.

Signature of Supervisor

Name: Dr Yeo Wei Hong

Date:

15/5/20